Pathological axonal enlargement in connection with amyloidosis, lysosome destabilization and hemorrhage is a major defect in Alzheimer's disease

Hualin Fu[1, 2, 3*], Jilong Li[1], Chunlei Zhang[1, 3], Guo Gao[1, 3], Qiqi Ge[2, 4], Xinping Guan[4, 5], Daxiang Cui[1, 3]

Affiliations:

[1]Institute of Nano Biomedicine and Engineering, School of Sensing Science and Engineering, School of Electronic Information and Electrical Engineering, Shanghai Jiao Tong University, 800 Dongchuan Road, Shanghai, 200240, China

[2]Institute of Marine Equipment, Shanghai Jiao Tong University, 211 Wenjin Road, Shanghai, 200240, China

[3]National Center for Translational Medicine, Shanghai Jiao Tong University, 800 Dongchuan Road, Shanghai, 200240, China

[4]Department of Automation, Shanghai Jiao Tong University, Shanghai 200240, China

[5]The Key Laboratory of System Control and Information Processing, Ministry of Education, Shanghai 200240, China

*Correspondence to: hfu@sjtu.edu.cn or 1010720220@qq.com (Hualin Fu)

Abstract: Alzheimer's disease (AD) is a multi-amyloidosis disease with Aβ deposits in the cerebral blood vessels, microaneurysms and senile plaques. How Aβ amyloidosis affects axon pathology is not well-examined. We studied Aβ-related axonal phenotypes with histochemistry, immunohistochemistry and fluorescence imaging methods. Widespread axonal amyloidosis with distinctive axonal enlargement was observed in AD. Aβ-positive axon diameters in AD brains were 1.72 times of control brain axons

by average. Axonal amyloidosis also associated with MAP2 reduction, Tau phosphorylation, lysosome destabilization and hemorrhagic markers such as ApoE, HBA, HbA1C and Hemin. Lysosome destabilization in AD was also clearly identified in the neural soma, associating with the co-expression of Aβ and Cathepsin D, HBA, ACTA2 and ColIV, implicating exogeneous hemorrhagic protein intake might influence neural lysosome stability. The data showed that Aβ-containing lysosomes were 2.23 times as large as the control lysosomes. Furthermore, under rare conditions, axon breakages were observed, which likely resulted in Wallerian degeneration. In summary, axonal enlargement associated with amyloidosis, chronic microhemorrhage and lysosome destabilization is a major defect in Alzheimer's disease.

Keywords: axonal enlargement; amyloidosis; lysosome destabilization; Aβ; Tau; hemoglobin; hemorrhage; Wallerian degeneration; neuropil thread; Alzheimer's disease

Introduction：

The pathological hallmarks of Alzheimer's disease include senile plaques, neurofibrillary tangles and neuritc dystrophy[1, 2]. Neuritc dystrophy refers to the dystrophy of axons and dendrites. In our previous investigation, we identified cerebral microaneurysm rupture and hemorrhagic Aβ leakage as a pathological mechanism for senile plaque formation[3]. Yet, how chronic hemorrhagic leakage impacts on other pathological phenotypes such as axonal dystrophy in Alzheimer's disease is not well-studied. Previous studies implicated that both Aβ and Tau phosphorylation are involved in the axonal defects in Alzheimer's disease[4-7]. However, the exact linkage between Aβ, Tau and their contribution to axonal dystrophy is still not very clear.

In the current study, we analyzed the pathological phenotypes in axons in AD brain tissues by immunohistochemistry, histochemistry and fluorescent imaging methods.

The results showed that the major axonal phenotype in Alzheimer's disease (AD) is the widespread axonal amyloidosis and enlargement with additional spheroid formation. The axonal defect in AD is associated with the enrichment of Aβ, phos-Tau, destabilized lysosomes and hemorrhage-related proteins in axons.

MATERIAL AND METHODS

Tissue sections. AD patient frontal lobe brain paraffin tissue sections were purchased from GeneTex (Irvine, CA, USA). Additionally, AD patient and non-AD control frontal lobe brain paraffin tissue sections were provided by National Human Brain Bank for Development and Function, Chinese Academy of Medical Sciences and Peking Union Medical College, Beijing, China. This study was supported by the Institute of Basic Medical Sciences, Chinese Academy of Medical Sciences, Neuroscience Center, and the China Human Brain Banking Consortium. All procedures involving human subjects are done in accord with the ethical standards of the Committee on Human Experimentation in Shanghai Jiao Tong University and in accord with the Helsinki Declaration of 1975.

List of antibodies for immunohistochemistry. The following primary antibodies and dilutions have been used in this study: Aβ (Abcam ab201061, 1 : 200, Cambridge, UK), Aβ/AβPP (CST #2450, 1 : 200, Danvers, MA, USA), phos-Tau (Abcam ab151559, 1:200), MAP2 (Proteintech 17490-1-AP, 1:200, Rosemont, IL, USA), ApoE (Abcam ab183597, 1:200), Sortilin1 (Abcam ab263864, 1:200), HBA (Abcam ab92492, 1:200), Cathepsin D (Abcam ab75852, 1:200), Lamp2 (Proteintech, 66301-1-Ig, 1:100), Cathepsin D (Proteintech 66534-1-Ig, 1 : 100), HbA1c (OkayBio K5a2, 1 : 100, Nanjing, Jiangsu, China), Hemin (Absolute Antibody, 1D3, 1 : 100, Redcar, UK), AGE (Advanced Glycation End Products) (Abcam, ab23722, 1:200), ColIV (Abcam ab236640, 1:200), ACTA2 (Proteintech 23081-1-AP, 1:400). The following secondary antibodies and dilutions have been used in this study: donkey anti-mouse Alexa-594 secondary antibody (Jackson ImmunoResearch 715-585-150, 1:400, West Grove, PA,

86 USA), donkey anti-rabbit Alexa-488 secondary antibody (Jackson ImmunoResearch
87 711-545-152, 1:400), donkey anti-rabbit Alexa-594 secondary antibody (Jackson
88 ImmunoResearch 711-585-152, 1:400), and donkey anti-mouse Alexa-488 secondary
89 antibody (Jackson ImmunoResearch 715-545-150, 1:400).
90
91 **Immunohistochemistry** was performed as described[8]. Briefly, paraffin sections were
92 deparaffinized by Xylene, 100% EtOH, 95% EtOH, 75% EtOH, 50% EtOH, and PBS
93 washes. Sections were then treated with 10 mmol/L pH 6.0 sodium citrate or 10 mmol/L
94 pH 9.0 Tris-EDTA antigen retrieval solutions in a microwave at high power for 5 min
95 to reach the boiling point and then at low power for another 15 min. The sections were
96 allowed to naturally cool down to room temperature. Then, the slides were blocked with
97 TBST 3% BSA solution for 1 hour at room temperature. After blocking, the samples
98 were incubated with primary antibodies at room temperature for 2 hrs followed by 5
99 washes of TBST. After that, the samples were incubated with fluorescent secondary
100 antibodies overnight at 4 degree. The treated samples were washed again with TBST 5
101 times the second day and mounted with PBS+50% glycerol supplemented with Hoechst
102 nuclear dye (Sigma, B2261, 1 μg/ml) and ready for imaging. IHC experiments without
103 primary antibodies were used as negative controls. All experiments have been repeated
104 in order to verify the reproducibility of the results.
105
106 **Rhodanine staining** was performed as described[3]. The Rhodanine staining kit
107 (BA4346) was purchased from Baso Diagnostics Inc. (Zhuhai, China). Briefly, paraffin
108 sections were first deparaffinized as described above. After a quick wash in 95%
109 ethanol, the slides were stained in the Rhodanine staining solution (0.01% p-
110 Dimethylaminobenzalrhodanine) in a 37-degree incubator for 30 minutes. After
111 staining, the slides were treated with a 95% ethanol quick wash and 5 times wash in
112 water, then mounted with PBS+50% glycerol solution for imaging analysis.
113
114 **Alizarin Red staining.** The Alizarin Red staining kit C0138 was purchased from
115 Beyotime Biotechnology (Shanghai, China). Briefly, paraffin sections were

deparaffinized as described above. Then, the slides were stained in the Alizarin Red staining solution (2% Alizarin Red, pH4.2) for 5 minutes at room temperature. After staining, the sections were washed 5 times with water, then mounted with PBS+50% glycerol solution for imaging.

Imaging and morphometry analysis. The fluorescent images were captured with a CQ1 confocal fluorescent microscope (Yokogawa, Ishikawa, Japan) and the color images of sections with histological stains were taken with an Olympus IX71 fluorescent microscope (Olympus Co., Toyoko, Japan). There is a difference in terms of exposure settings when imaging axonal staining versus senile plaque staining. To image axonal Aβ staining clearly, the exposure time should be increased significantly. Images were then analyzed with ImageJ software (NIH, USA). When comparing signal intensities with the same exposure settings, the mean area density was used as the parameter to define the marker densities. The perimeters of axons in transverse orientations were measured to simplify the axon diameter estimation by using the following formula: diameter = perimeter/3.14. The diameters of axons could also be measured directly with the ImageJ line tool utilizing the microscopy scale as a reference.

Statistics. All data first went through a Shapiro & Wilk normality test using SPSS Statistics 19 software. Two-tailed unpaired T-test was used to compare the means of data with a normal distribution with Excel 2007 software. For data that were not normally distributed, nonparametric Mann-Whitney test was performed to compare the means by using SPSS Statistics 19 software. For the correlation analysis, Pearson correlation was used for the data with a normal distribution while Spearman correlation was used for the data that were not normally distributed. The p Value threshold for statistical significance is set at 0.05. If $p<0.05$, then the difference was considered statistically significant. When $p<0.001$, it was labeled as $p<0.001$. If $p \geqq 0.001$, then the p Value was shown as it was.

Funding: This work was supported by the National Natural Science Foundation of

China (81472235), the Shanghai Jiao Tong University Medical and Engineering Project (YG2021QN53, YG2017MS71), the International Cooperation Project of National Natural Science Foundation of China (82020108017), and the Innovation Group Project of National Natural Science Foundation of China (81921002).

Author contributions: HF conceived the study, designed and supervised the experiments and wrote the manuscript; HF, JL performed the experiments; HF, JL, CZ, GG, QG, XG and DC did the data analysis; all authors reviewed the manuscript.

Competing interests: Authors declare no competing interests.

Data availability statement: The data that supports the findings of this study are available from the corresponding author upon request.

Supplementary Materials. Supplementary Figures 1 to 11.

Results:

Axon amyloidosis and enlargement in AD brain tissues

In our previous publications, Aβ staining was detected in senile plaques, CAA, neurons and red blood cells[3, 9]. After careful re-examination of the Aβ staining patterns in AD brain sections with optimized staining conditions and longer exposure settings, we found that there were clear axon-specific Aβ staining patterns that we previously did not recognize (two overview images of Aβ staining of AD axons in the longitudinal and transverse orientation were displayed in Supplementary Figure 1 and 2). The axon fragments we focused on in this study are mainly axons in the gray matter or at the gray matter/white matter boundary, which could be defined as proximal axons that are close to the neuron soma. The study extended the analysis to axons in the white matter since many aspects of the axon fragments in the white matter showed similar changes as the

proximal axons. Figure 1A and Supplementary Figure 1, 2 showed that axon amyloidosis is widespread in AD brain tissues. Aβ immunostaining was distributed along the length of many axons. Aβ-positive axons can be observed both around senile plaques and without senile plaques in the vicinity. Axonal amyloidosis could be detected in axons at both longitudinal and transverse orientation. Axons with Aβ staining were often shown as grouped clusters, corresponding to the known structural character in the human brain cortex as "axon bundles". Axon bundle, or in the name of "axonal tract" [10] were frequently observed in the Layer VI of the cerebral cortex, which was at the boundary of grey matter/white matter formation. An image of MAP2-labeled axon bundles in the control brain was shown in the Supplementary Figure 3. To our knowledge from the literature, "axon bundles" derived from the neurons is the only type of neural cell processes that shows a "bundling" phenotype, different from astrocyte or microglial processes (Supplementary Figure 4). These intracortical axon bundles had an average transverse diameter of 61.61±9.88 um (N=11). Each bundle contained an average of 19.09±4.61 axons per area (N=11) (Supplementary Figure 3). The enlarged and often bundled axons but not unaffected axons in AD brain tissues could also be clearly identified with phase contrast microscopy because they have enhanced contrast and are darker in appearance. These enlarged axons were not labeled with microglial marker Iba1 or astrocyte marker GFAP (Supplementary Figure 4). Additionally, the enlarged axons could be identified with an alternative marker of amyloidosis other than Aβ antibody staining, the amyloid blue autofluorescence[11, 12], which we referred to a term of "MetaBlue" in the previous studies[3, 9]. From cortical surface to white matter, axon bundles at transverse orientation or longitudinal orientation could be observed within a same pathological section indicating different populations of axon bundles (Supplementary Figure 1, 2, 3). Axon bundles were most clearly observed in Layer VI of the brain cortex, showing as long axon fragments that bundled together.

Moreover, puff-like spheroid formation can be detected in a subset of the Aβ-positive

205 axons. Spheroids are often formed at positions with further-enhanced Aβ staining. Aβ-
206 positive axons have a general enlargement phenotype (Figure 1B), which is a basic
207 character appearing more frequently than the spheroid formation. Topologically,
208 "spheroid" could be viewed as an extreme form of "enlargement". The slight difference
209 of " enlargement" vs "spheroid" in describing axonal defects could be analogous to the
210 concept of "fusiform" or "saccular form" when describing "aneurysm". The diameters
211 of Aβ-positive axons in the transverse orientation outside of senile plaque regions were
212 measured since the strong plaque Aβ staining precludes the accurate identification of
213 Aβ-positive axons within the senile plaques. The measured Aβ-positive proximal axons
214 had an average diameter of 1.94±0.59 μm (N=200) while MAP2-labeled proximal
215 axons from control front brain samples measured around 1.13±0.39 μm (N=34). In
216 another word, Aβ-positive axon diameters were around 1.72±0.52 fold of control axons
217 (Mann Whitney test, $p<0.001$). In addition, among AD axon samples, the mean Aβ
218 staining intensity was weakly positively related to the axon diameter ($r=0.338$, $p<0.001$,
219 N=200, Spearman correlation), further emphasizing the positive influence of Aβ on the
220 size enlargement of axons. When axons in the white matter were analyzed, MetaBlue-
221 positive amyloid-laden axon diameters were around 3.80±0.69 μm (N=100), showing
222 even more severe enlargement than the proximal axons in the gray matter or at the gray
223 matter/white matter boundary. The data suggested that the Aβ-amyloidosis-associated
224 axonal enlargement is a basic pathological phenotype in Alzheimer's disease.
225

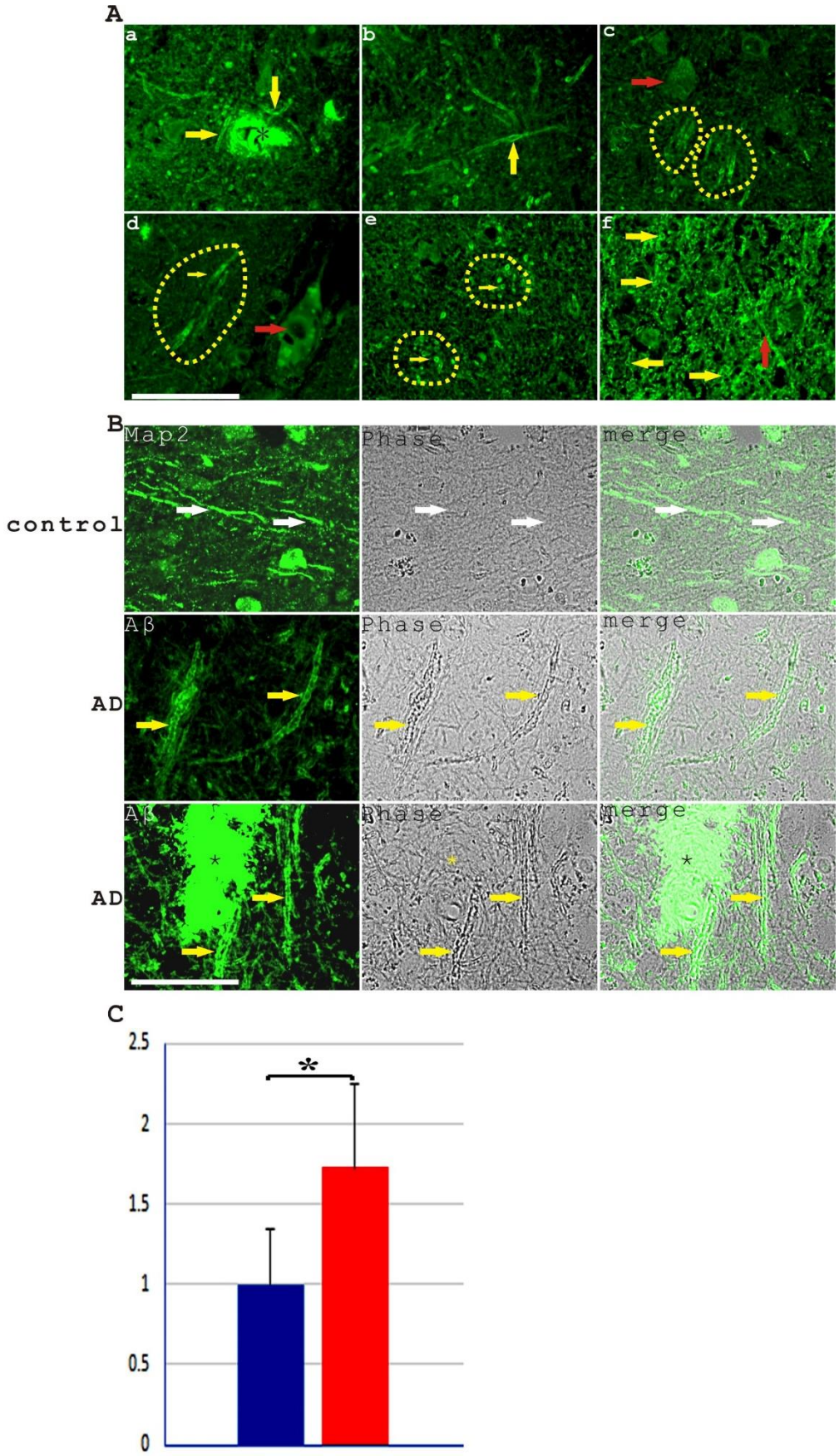

226

227 **Figure 1: Axon amyloidosis and enlargement are important pathological**

phenotypes in Alzheimer's disease. A. Axon amyloidosis was detected in AD frontal brain tissues with Aβ antibody with green fluorescence. **a**, Aβ expression was detected both in a senile plaque (indicated with an asterisk) and in axons (indicated with arrows). **b**, An axon at the longitudinal orientation showed spheroid formation stained with Aβ antibody (indicated with an arrow). **c**, Two clusters of Aβ-positive axons in the longitudinal direction (indicated by dashed lines) were shown, indicating Aβ staining of axon bundles. An Aβ-containing neural cell was indicated with a red arrow. **d**, A cluster of Aβ-positive axons in the longitudinal direction (indicated by dashed lines) was shown while blood vessel lumen Aβ expression was indicated with a red arrow. **e**, Two clusters of Aβ-positive axons in the transverse direction (indicated by dashed lines) were shown while individual axons were indicated by yellow arrows. **f,** Axons with abundant axonal Aβ staining mostly in the transverse direction (yellow arrows) were observed in the white matter with one longitudinal axon indicated by a red arrow. Scale bar, 50 μm. **B**. A general enlargement of axons in AD brain tissues was observed when comparing control axons (indicated by white arrows, top panel) marked by MAP2 antibody staining to amyloid-loaded axons in AD (indicated by yellow arrows, bottom two panels) marked by Aβ immunostaining. A senile plaque in the bottom panel was labeled with an asterisk. Scale bar, 50 μm. **C**. Imaging measurements showed that Aβ-positive axons had an average diameter of 1.94±0.59 μm (N=200) while MAP2-labeled control axons measured around 1.13±0.39 μm (N=34). Aβ-positive axons were significantly enlarged, averaging 1.72±0.52 fold of control axons ($p<0.001$, Mann-Whitney test).

Axons in AD patients showed a reduction of structural protein MAP2

To examine the effect of axon amyloidosis on the neurons, AD brain sections was stained with the antibody against MAP2, a microtubule-associated structural protein highly expressed in the neuron soma, dendrite and axon. It has been shown that MAP2 labels the neuronal cell soma, dendrites and axons with hippocampal neuron culture or N2a cell line cell culture models [13, 14]. MAP2 is also a good marker for axons in

258 pathological studies, which has been applied successfully in rat brain traumatic axonal
259 injury model studies [15-17]. Although some cell culture experiments suggested that
260 MAP2 is a proximal-axon-restricted marker in cultured dorsal root ganglion sensory
261 neurons[18], however, if looking at the published data carefully, MAP2 expression is
262 not confined to the proximal axons but also extended along the length of axons. MAP2
263 staining pattern might be very sensitive to experiment conditions given its profound
264 changes during neurodegeneration. Different *in vivo* or *in vitro* experiment conditions
265 such as different cell types, cell culture and cell growth conditions or staining of
266 different MAP2 isoforms might explain the heterogeneity of the MAP2 staining results.
267 In our immunostaining experiments on AD brain pathological sections and control brain
268 sections, MAP2 stained the neuron soma and axons strongly and was clearly expressed
269 in Layer VI axon bundles and in the axons in the white matter (Figure 1, 2 and
270 Supplementary Figure 3), which proved that MAP2 is a useful marker for axon analysis
271 in human brain pathology studies. The presented image showed that there was a
272 significant decrease of signals of MAP2-stained axons (MAP2-positive axon numbers
273 decreased more than half, at around 53.4% when examining from the longitudinal
274 orientation（the top panel of Figure 2A). The counting from the transverse orientation
275 image displayed even larger decrease around 79.8% of axon MAP2 signals (the bottom
276 panel of Figure 2A). Double immunostaining with Aβ antibody showed that MAP2
277 expression inversely correlated with Aβ staining on the axons in AD brain tissues
278 (Figure 2B). In AD brain white matter, many axons presented a decrease of MAP2
279 protein while bearing significant Aβ staining. MAP2 staining on Aβ-positive axons was
280 often fragmented and diffusive. Within dense-core senile plaques, there is usually very
281 little MAP2 immunostaining. The reduced MAP2 expression in amyloid-laden axons
282 in the white matter could also be observed when using amyloid blue autofluorescence
283 as an axon amyloidosis marker (Figure 2C). It is estimated, based on one set of
284 experiments, Aβ immunohistochemistry labeled proximal axons around 44.2% by
285 counting the average number of Aβ-labeled axons per axon bundle at transverse
286 orientation (8.44±4.10, N=16) and divided by the average axon bundle axon number of

287 19.09 in control samples, which we obtained earlier. Axons with amyloid blue
288 autofluorescence showed much weaker MAP2 intensity (0.36±0.07, N=100) comparing
289 to axons without amyloid blue autofluorescence (N=25). In another word, amyloid-
290 laden axons lost MAP2 expression at an average rate of 64% in the white matter.
291 Besides the decrease of MAP2 protein in axons, reduced MAP2 immunostaining
292 intensity in the neuron soma was also observed in neurons with intracellular Aβ
293 (Supplementary Figure 5), suggesting that Aβ could have a deleterious effect on MAP2
294 expression both in the axons and in cell bodies.

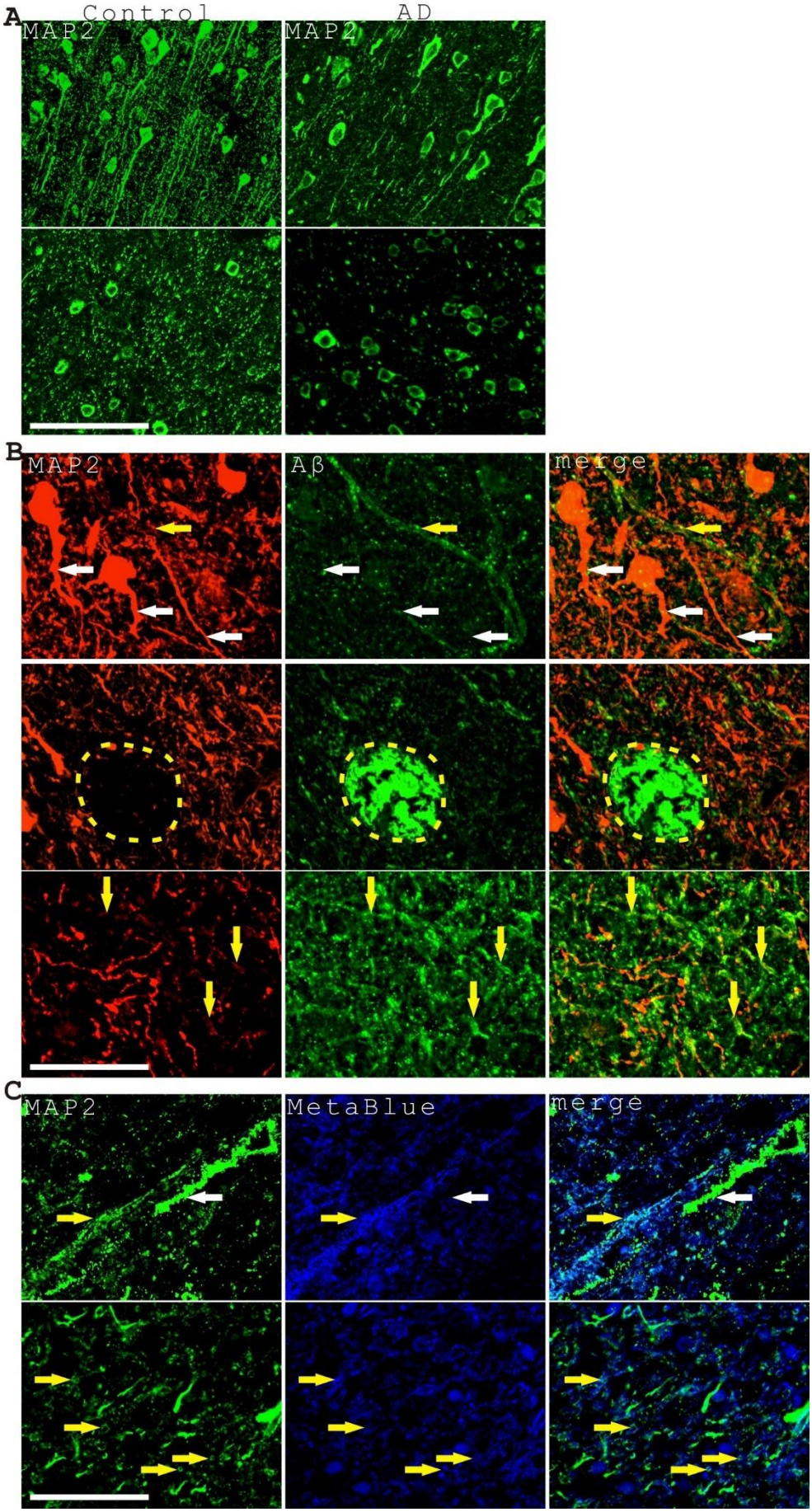
A
Control
AD
MAP2
MAP2
B
MAP2
Aβ
merge
C
MAP2
MetaBlue
merge

296 **Figure 2. Axons in AD frontal brain tissues showed a decrease of axon structural**
297 **protein MAP2. A**. At longitudinal (top panel) and transverse orientation (bottom panel),
298 a significant decrease of MAP2-positive axons in AD brain tissues comparing to control
299 brain tissues was observed. The top panel showed that there were 26 long MAP2-
300 positive axon fragments in the control sample while only 12 long MAP2-positive axon
301 fragments in the AD sample, indicating a 53.8% decrease. The bottom panel showed
302 there were around 391 strong MAP2-positive axon dots in the control brain while there
303 were around 79 strong MAP2-positive axon dots in AD brain, which indicated a 79.8%
304 decrease. Scale bar, 100 μm. **B.** Four representative images showed that the decrease of
305 axonal MAP2 signals was correlated with increased Aβ immunostaining in axons in AD
306 brain tissues. The top three images showed axons in the grey matter with greatly
307 reduced MAP2 staining (amyloid-laden axons were indicated with yellow arrows while
308 unaffected axons were indicated with white arrows). The yellow dashed-lines in the
309 third image circled a dense-core senile plaque with barely detectable MAP2
310 immunostaining. The bottom image showed many Aβ-loaded axons with diminished
311 MAP2 staining in the white matter. Scale bar, 50 μm. **C**. Two representative images
312 showed greatly reduced axonal MAP2 staining in amyloid-laden axons labeled with
313 amyloid blue autofluorescence in the white matter. The top panel showed axons mostly
314 in the longitudinal direction and the bottom panel showed axons mostly in the
315 transverse direction. The yellow arrows indicated the amyloid-loaded axons while the
316 white arrow indicated a control axon without blue autofluorescence. Axons with
317 amyloid blue autofluorescence showed much weaker MAP2 intensity (0.36±0.07,
318 N=100) comparing to axons without amyloid blue autofluorescence (N=25). Scale bar,
319 50 μm.
320
321 **Lysosomal destabilization was detected in AD frontal brain tissues**
322
323 We hypothesized that the decrease of MAP2 protein in axons might be due to some
324 faulty protein degradation events although other mechanisms such as the reduction of
325 MAP2 mRNA transcription or protein synthesis are also possible. Lysosomes and

326 proteasome pathway are major pathways of protein degradation. Since we observed that
327 Aβ-positive axons appear to contain many vesicles, we stained the sections with
328 lysosomal enzyme marker Cathepsin D. Although previously we identified some weak
329 extracellular Cathepsin D staining coming together with senile plaque Aβ aggregates,
330 we also observed intracellular neuronal lysosome Cathepsin D staining clearly[3].
331 However, neuronal Cathepsin D staining was not homogeneous. Instead, we frequently
332 observed abnormal Cathepsin D staining in the senile plaque regions (Figure 3). Normal
333 lysosomal staining showed granule-like patterns with strong Cathepsin D signals.
334 Conversely, nearly half of the lysosomal compartments in senile plaques showed
335 abnormal Cathepsin D staining with enlarged, diffusive and weak staining patterns,
336 indicating lysosomal destabilization, which has also been studied in previous
337 literatures[19-21]. A weak but detectable Aβ staining could be observed in these
338 abnormal lysosomal compartments. We measured the sizes and intensities of lysosomal
339 compartments within senile plaque regions comparing to lysosomes outside of senile
340 plaque regions. The lysosomal compartments (including all Cathepsin D-labeled
341 compartments) within the senile plaques are roughly 4.32±1.99 μm (N=122) in size,
342 which is 3.65±1.68 (Mann Whitney test, $p<0.001$) times of control lysosomes outside
343 of plaque regions (1.18±0.39 μm, N=60) and characterized by considerably weaker
344 Cathepsin D staining intensity (0.76±0.3) (Mann Whitney test, $p<0.001$). In AD axons,
345 Aβ and lysosomal enzyme marker Cathepsin D are highly co-localized, showing the
346 predominant presence of axonal Aβ in the lysosomes. We also detected diffusive and
347 weaker Cathepsin D staining patterns along the length of Aβ-positive axons, suggesting
348 axonal lysosome destabilization was happening (Figure 3D-F). Control cellular
349 lysosomes far away from senile plaques had strong, clear granule-like Cathepsin D
350 staining patterns (Figure 3G). Additional evidence showing axonal amyloidosis
351 associating with unusually diffusive Cathepsin D staining was presented in
352 Supplementary Figure 6. Amyloid blue autofluorescence was used as an amyloidosis
353 marker in this figure instead. However, lysosome destabilization was not limited to
354 axons, when looking at intracellular lysosomes more carefully, many neural cells also
355 revealed heterogeneous Cathepsin D staining patterns, which were presented further in

Figure 4. To summary, we think that the destabilized lysosomes might be related to the decrease of MAP2 protein in the axons.

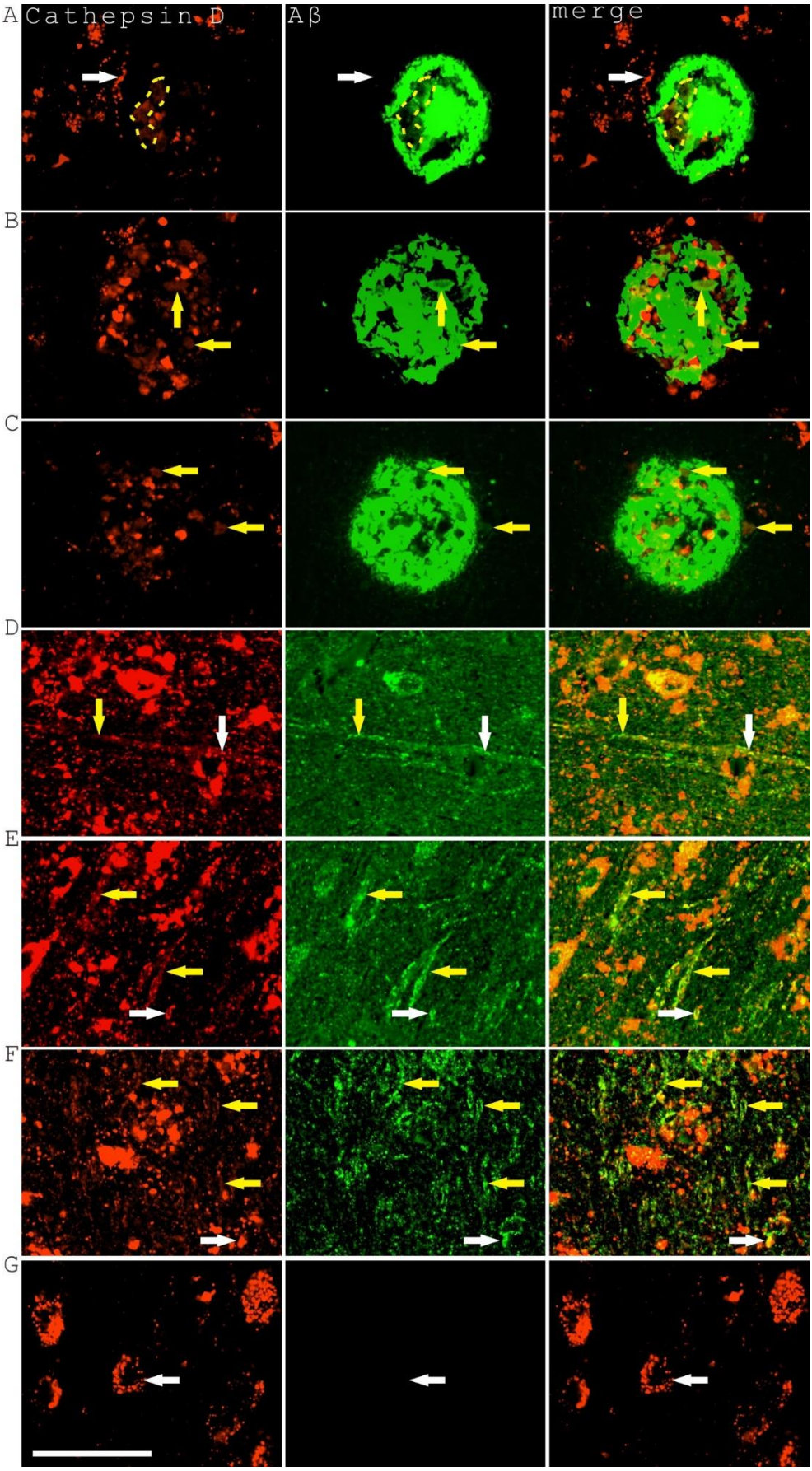

360

361

362 **Figure 3. Lysosomal destabilization was common in AD frontal brain tissues.** Three
363 representative plaques were shown associating with lysosome destabilization (**A-C**).
364 The top plaque was a typical dense-core plaque while the bottom two plaques were
365 more diffusive. All three plaques associated with enlarged and diffusive Cathepsin D
366 staining patterns (yellow dashed lines or yellow arrows), a character of lysosome
367 destabilization and lysosome permeabilization comparing to typical, granule-like
368 strong lysosome staining with focal Cathepsin D positivity (indicated with white arrows
369 in the top panel). Weak Aβ staining could be observed in these abnormal lysosomal
370 compartments. (**D-F**) showed three representative images illustrating the diffusive
371 Cathepsin D staining in the Aβ-positive axons (indicated with yellow arrows). At the
372 same time, the co-localization between Aβ and Cathepsin D in lysosomes was
373 abundantly observed (indicated with white arrows). It should be noted that these three
374 pictures were taken with longer exposure settings in order to show the weak axonal Aβ
375 and Cathepsin D staining comparing to other pictures. **G**. Intracellular lysosomes away
376 from amyloid plaques showed mostly clear, strong and granule-like lysosomal
377 Cathepsin D staining (indicated with white arrows). Scale bar, 50 μm.
378
379 Lysosomes are abundantly present in the neuronal soma. If lysosome destabilization is
380 happening surrounding senile plaques, we should also expect to see some destabilized
381 lysosomes in the cell bodies. Not surprisingly, we did observe frequent lysosomal
382 destabilization in Aβ-containing neural cells (Figure 4 and Supplementary Figure 7).
383 We use neural cells with little Aβ staining as internal controls for unaffected lysosomes
384 (Figure 4A). The control lysosomes appeared normal-looking with punctuate, compact
385 staining of Cathepsin D. In cells with abundant Aβ signals, lysosomes became enlarged,
386 clustered and their Cathepsin D staining became diffusive. The enlargement of
387 lysosomes filled with Aβ could be observed at single lysosome level (yellow arrows in
388 Figure 4B, 4C). The Aβ-loaded and enlarged lysosomes often clustered with each other
389 to form large lysosomal domains with diffusive Cathepsin staining (Figure 4D, E).
390 Quantitatively, Aβ-containing lysosomes (N=30) had an average size 1.63±0.27 μm,
391 which is 2.23±0.38 times (the difference is statistically significant with $p<0.001$, T-test)

of control lysosomes with no Aβ staining with the average size of (0.73±0.09 μm, N=12) and an average intensity of 0.32±0.12 times ($p<0.001$, Mann-Whitney test) of control lysosomes, demonstrating that Aβ-associated lysosome destabilization is a distinctive phenotype of intracellular amyloidosis. We also observed that Aβ staining sometimes showed up at extra-lysosomal locations in the cytoplasm or even in the nucleus. Occasionally, we also observed Cathepsin D staining in the nucleus (Figure 4F, G). The existence of Aβ and Cathepsin D in locations other than lysosomes might also be related to lysosome destabilization and leakage, which theoretically could relocate lysosomal contents to other cellular compartments.

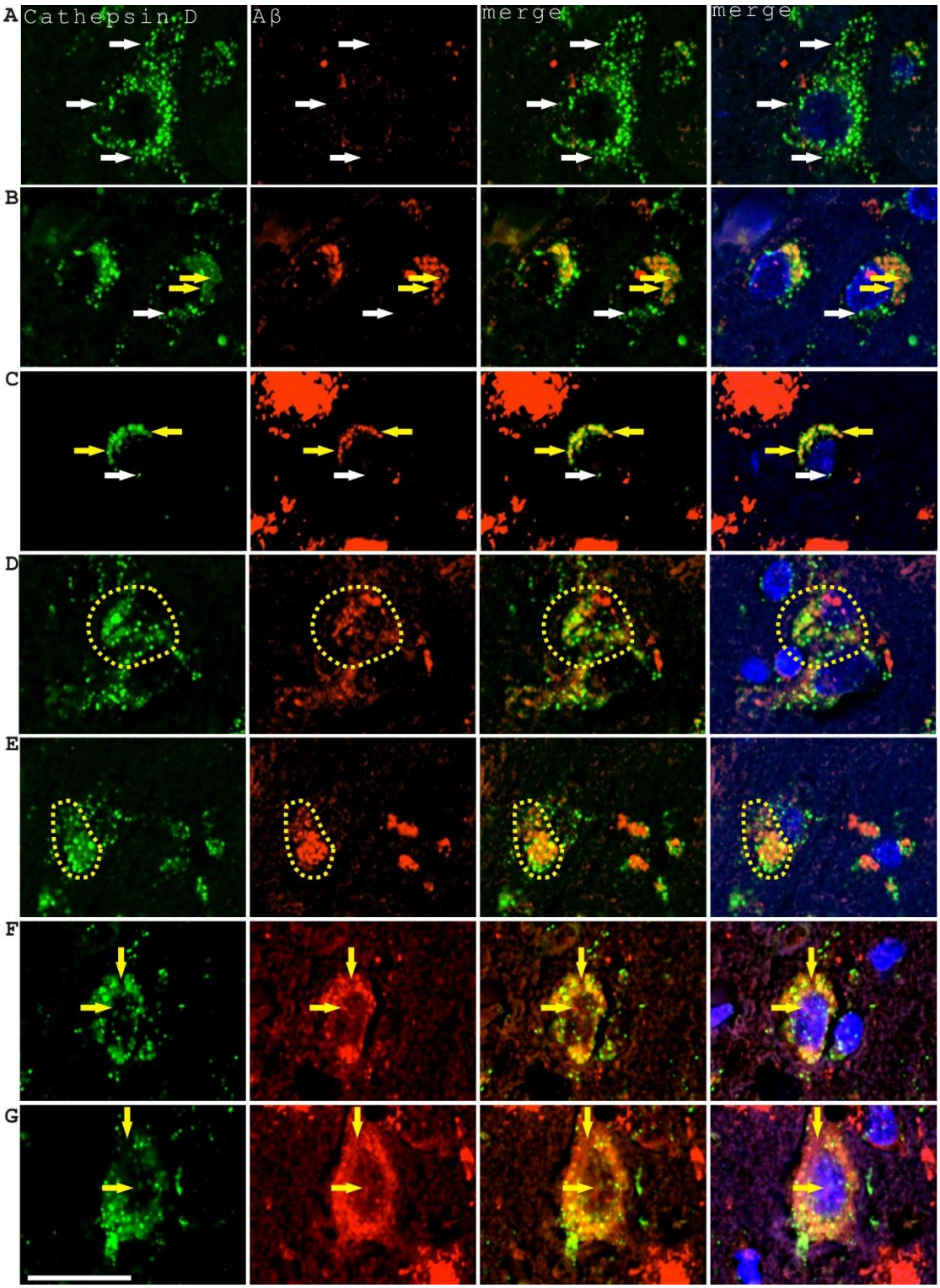

Figure 4. Lysosomal destabilization highly associated with Aβ in the cell bodies of neural cells in AD frontal brain tissues. A. A control neural cell with little Aβ staining showed mostly normal lysosome Cathepsin D staining patterns (indicated with white arrows). **B, C.** Intracellular Aβ associated with lysosome destabilization, which could be identified at single lysosome levels with significant lysosome enlargement and

409 diffusive staining (indicated with yellow arrows) while control lysosomes indicated
410 with white arrows showing compact and bright Cathepsin D staining. **D, E** showed two
411 representative images indicating that intracellular Aβ expression associates with
412 lysosome enlargement, clustering and diffusive staining. **F**, **G** showed two
413 representative images of neural cells containing not only lysosomal Aβ and Cathepsin
414 D but also extra-lysosomal Aβ, nuclear Aβ and Cathepsin D. The vertical arrows
415 indicated Aβ staining outside of Cathepsin D-stained areas while the horizontal arrows
416 indicated nuclear Aβ and Cathepsin D staining. Quantitative measurement showed that
417 Aβ-containing cell body lysosomes (N=30) had an average size of 1.63±0.27 μm, which
418 is 2.23±0.38 times of control lysosomes without Aβ staining (0.73±0.09 μm, N=12) and
419 an average Cathepsin D intensity of 0.32±0.12 time of control lysosomes. Scale bar, 25
420 μm.
421
422 The above result strengthened the concept of lysosome destabilization in AD as also
423 reported from previous studies [20-23], which can be regarded as a consensus in the
424 field. However, whether abnormal lysosomes produced Aβ or Aβ induced lysosomal
425 destabilization is still a debated issue. Nevertheless, we could tackle this difficult
426 question in some way by studying the molecules interacting with Aβ. Previously, we
427 established a linkage between Aβ senile plaque formation and intravascular hemolysis,
428 vascular degeneration and microaneurysm rupture[3, 9]. The relationship between
429 microhemorrhage and Aβ senile plaque information has also been explored in other
430 published investigations[24-30]. Thus, Aβ might interact with hemolysis or vascular
431 markers either directly or indirectly, which should be reflected with the co-distribution
432 of Aβ with hemolytic or vascular markers. We analyzed the intracellular co-expression
433 of a hemolysis-related marker HBA (alpha Hemoglobin) and two vascular-related
434 markers ACTA2 and ColIV with Aβ (Figure 5). All three markers showed good co-
435 localization with intracellular Aβ in lysosome-like structures. HBA and ACTA2 signals
436 as well as Aβ signals were also frequently observed in the nucleus (Figure 5A). When
437 we performed HBA and Cathepsin D double-immunostaining on AD sections, the co-
438 distribution of HBA signals with destabilized lysosomes as indicated with enlarged and

clustered lysosome compartments and diffusive Cathepsin D staining was also observed (Figure 5B). This indicated that the protein partners interacting with Aβ such as HBA also associated with lysosome destabilization in neural cells.

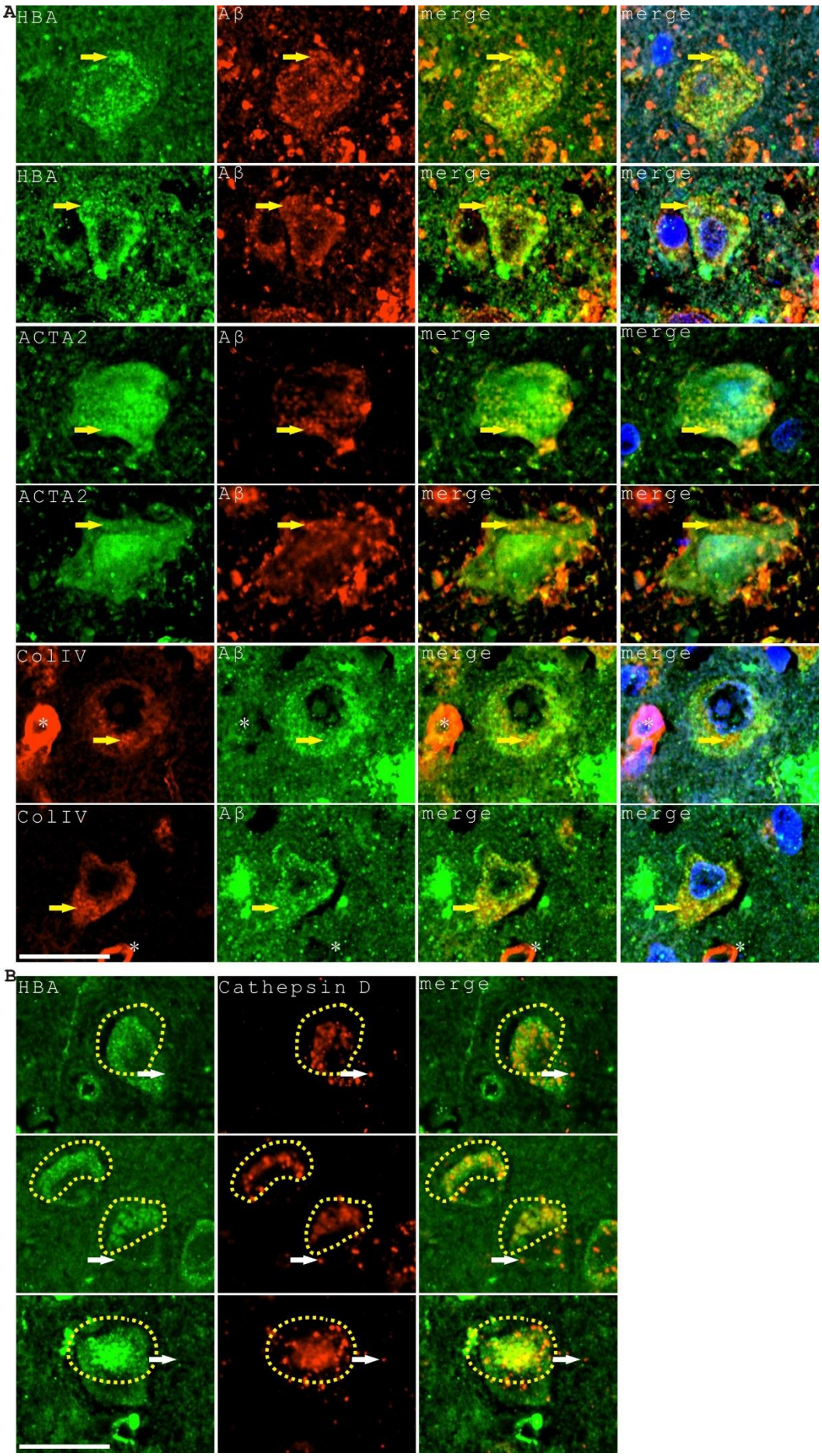
A
HBA
Aβ
merge
merge
HBA
Aβ
merge
merge
ACTA2
Aβ
merge
merge
ACTA2
Aβ
merge
merge
ColIV
Aβ
merge
merge
ColIV
Aβ
merge
merge
B
HBA
Cathepsin D
merge

Figure 5. Blood and vascular proteins co-existed with intracellular Aβ in neural cells in AD frontal brain tissues and might also be related to lysosome instability. **A**. Representative images showing the co-expression of blood related marker HBA, vascular related markers ACTA2, ColIV and Aβ. The co-localization of markers was indicated with yellow arrows. Two small blood vessels were indicated with asterisks in the ColIV staining panel. **B**. The intracellular HBA expression domains overlapped with the region of lysosomal destabilization indicated with enlarged and clustered lysosomal compartments and diffusive Cathepsin D staining (marked with yellow dashed circles). Control HBA-unaffected lysosomes were indicated with white arrows. Scale bars, 25 μm.

Destabilized lysosomes existed in dystrophic neurites

It is clear that there is a lysosome destabilization phenotype in neuronal cells associating with intracellular Aβ from studies above. Since we focused more on the axonal phenotype in AD, to further verify if destabilized lysosomes were linked to axon degeneration, we stained the tissue sections with phosphorylated Tau (phos-Tau) antibody, a well-known axon dystrophy marker in Alzheimer's disease, and the lysosomal membrane marker Lamp2. The localization of abnormally diffusive lysosomal Lamp2 staining in phos-Tau-positive dystrophic neurites, neurofibrillary tangles, axons and neuropil threads was observed (Figure 6A). In addition, the abnormally diffusive lysosomal Lamp2 staining in phos-Tau-positive dystrophic axons was also abundantly detected in the white matter (Figure 6A, bottom panel). Neuropil thread is a collective term traditionally used for phos-Tau staining in both axons and dendrites. We noticed that, across broad brain regions, neuropil thread phos-Tau staining was more abundant than phos-Tau staining of the tangles and senile plaque dystrophic neurites (Supplementary Figure 8). phos-Tau positive neurites in AD tissues could be classified with primary dystrophic neurites at an average diameter of 1.56±0.37 μm (N=40) or secondary dystrophic neurites with an average diameter of 0.40±0.09 μm (N=30) based on their diameters, which might reflect the different size

473 of axons or dendrites. When we stained AD brain sections with both phos-Tau and Aβ
474 antibodies, the co-localization between phos-Tau and Aβ was also detected in
475 dystrophic neurites in senile plaques, neurofibrillary tangles, neuropil threads and axons
476 (Figure 6B). However, Aβ staining in dystrophic neurites, tangles and axons was lower
477 comparing to the strong Aβ staining in the senile plaques. These data confirmed that
478 axon dystrophy connected with Aβ, Tau phosphorylation and lysosome destabilization.

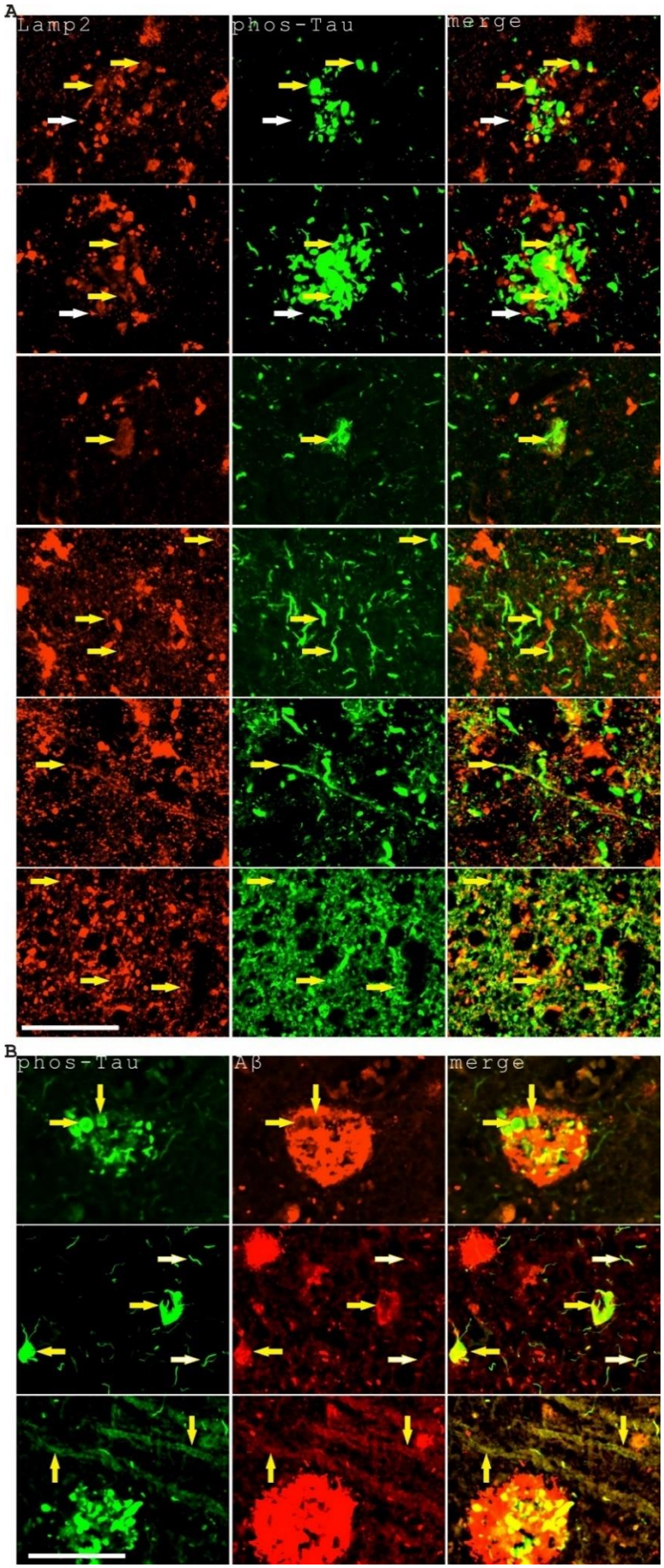
A
Lamp2
phos-Tau
merge
B
phos-Tau
Aβ
merge

Figure 6. Destabilized lysosomes were located in AD frontal brain dystrophic neurites, tangles, axons and neuropil threads, additionally there is a co-distribution between phos-Tau and Aβ in dystrophic neurites, tangles, neuropil threads and axons. A. Abnormal lysosome Lamp2 staining (indicated with yellow arrows) was detected in peri-plaque dystrophic neurites (top two panels), a representative tangle (the third panel), a representative longitudinal axon (the fourth panel) and white matter axons mostly in the transverse direction (the bottom panel) marked with phos-Tau immunostaining. We observed long, diffusive but relatively weaker Lamp2 staining along the length of axons and neuropil threads, highlighting the intricacy of this defect. The bottom three picture was taken with longer exposure time settings in order to show the relatively weak signals in neuropil threads and axons. Control lysosomes not affected by Tau phosphorylation were indicated with white arrows. Scale bar, 50 μm. **B**. phos-Tau-positive dystrophic neurites (yellow arrows, top panel), tangles (yellow arrows) and neuropil threads (white arrows) (middle panel) and axons (yellow arrows, bottom panel) were also Aβ-positive. Scale bar, 50 μm.

Axon degeneration in AD bears the markers of hemorrhagic insults

It is not very clear why cells and axons in AD tissues are degenerating. A lysosome destabilization mechanism was proposed initially based on cell culture studies [20, 21]. However, in the *in vivo* situations, Aβ alone might not be fully responsible for the degenerating effect since Aβ is interacting with many other proteins. As our previous research suggested that senile plaques are formed by blood Aβ leakage into the brain upon microaneurysm rupture, we hypothesized that axon damages in AD tissues might be also associated with many blood-related proteins. We checked the axon pathology with a variety of blood or plasma-related markers. The results showed that enlarged axons in AD brains indeed carried blood and plasma markers such as ApoE, HBA, HbA1C and Hemin (Figure 7A-D). Overt acute hemorrhage was rarely observed surrounding these affected axons, suggesting that the intake of hemorrhagic markers in these axons is likely a chronic event. It appears that the presence of blood markers in

510 the axons is not depending on the spatial closeness to the senile plaques. In addition,
511 the distribution of hemorrhagic markers is not always quantitatively proportional to the
512 intensity of Aβ in AD brain tissues. Sometimes there is even stronger staining of
513 hemorrhagic markers in the axons than in the surrounding senile plaques, which is
514 likely because of the differential enrichment or metabolism of amyloid protein
515 complexes in axons vs. senile plaques (an example was shown in the top panel of Figure
516 7D with more Hemin staining in the axons than in the adjacent senile plaque). Moreover,
517 axon amyloidosis is associated with the expression of Sortilin1, another
518 endosomal/lysosomal marker (Figure 7E), which has also been implicated as a major
519 receptor for ApoE and a component of senile plaque[31, 32]. Since intracellular Aβ
520 mostly existed in the lysosomes as shown in Figure 3, the above data also suggested
521 that intracellular ApoE, HBA, HbA1C and Hemin primarily located in the lysosomes.
522 An overview image of widespread HBA and Aβ expression in the white matter axons
523 was further presented in the Supplementary Figure 9. Additionally, when we stained the
524 sections with red blood cell related histological stains such as Alizarin red and
525 Rhodanine[3], we could also see many axons in AD brain tissues positively stained by
526 these stains (Supplementary Figure 10). Actually, AD white matter is broadly stained
527 with Alizarin red and Rhodanine, similarly as HBA, showing an extensive effect of
528 hemorrhagic markers on the white matter axons. All these analyses indicated that the
529 axons not only were enriched for Aβ but also enriched for many hemorrhage-related
530 markers.

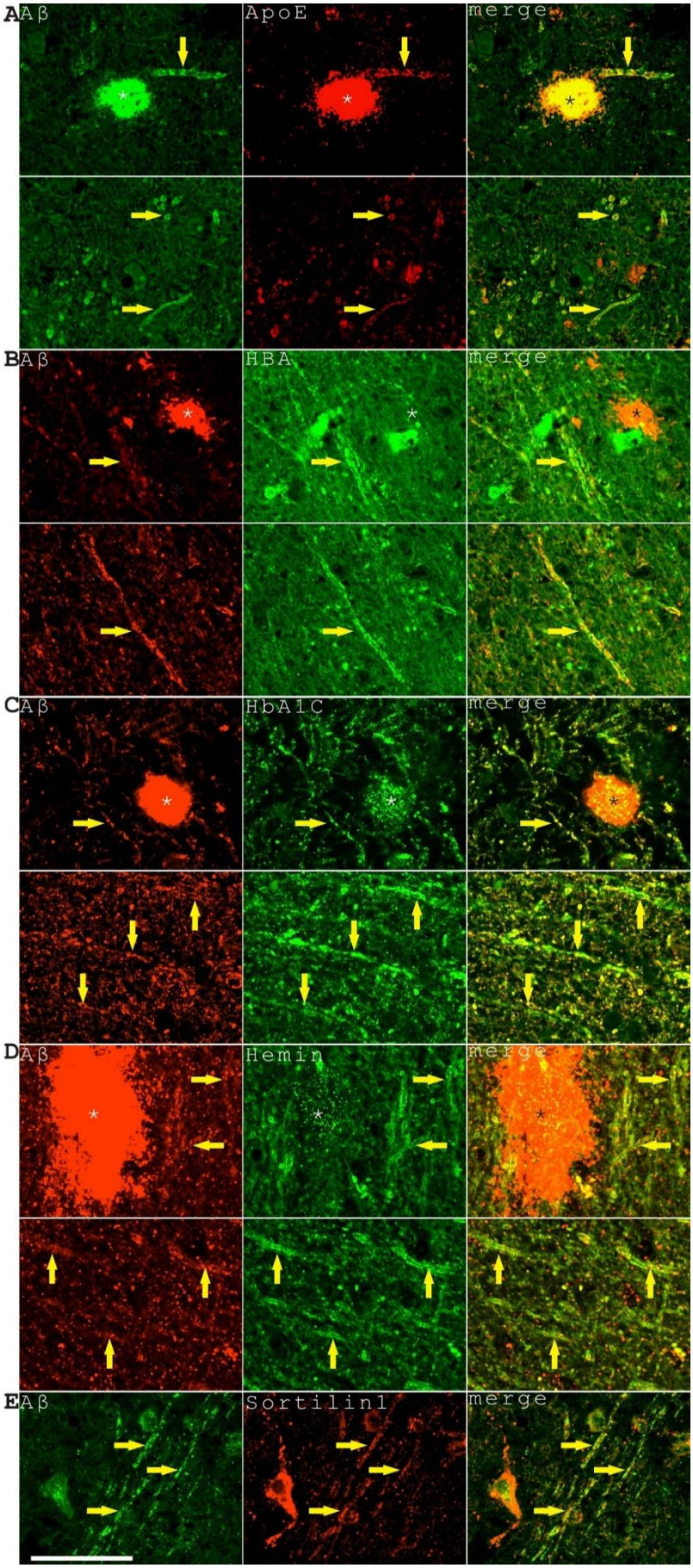
A
Aβ
ApoE
merge
B
Aβ
HBA
merge
C
Aβ
HbA1C
merge
D
Aβ
Hemin
merge
E
Aβ
Sortilin1
merge

531

532 **Figure 7. Axon degeneration in AD bears the markers of hemorrhagic insults in**
533 **AD frontal brain tissues.** Four blood-related markers (ApoE, HBA, HbA1C, Hemin)
534 all showed positivity in enlarged axons labeled with Aβ immunostaining, that can be
535 adjacent to senile plaques (top image in each panel) or not associated with senile
536 plaques (bottom image in each panel) (**A** to **D**). Degenerating axons were also positive
537 for an endosomal/lysosomal marker Sortilin1 (**E**). The affected axons were indicated
538 by arrows while the senile plaques were indicated with asterisks. Scale bar, 50 μm.
539
540 **Under rare occasions, axon breakages were observed in AD brain tissues**
541
542 Whether the axonal degeneration defects will ultimately lead to axon breakages in
543 Alzheimer's disease is an important question to be addressed. We checked hundreds of
544 images containing Aβ-stained axons. We initially focused on axons traveling in the
545 longitudinal orientation inside of senile plaques since the axons in the transverse
546 orientation were difficult to be individually identified. We observed that many axons
547 passing through the senile plaques were Aβ-positive and enlarged but they did not break
548 (Supplementary Figure 11). However, we did find a few examples indicating that the
549 axons could truly be broken at locations outside of senile plaques. Using Aβ and AGE
550 antibody as the markers for amyloidosis-affected axons, broken axons with gaps up to
551 38.4 μm in width could be detected (Figure 8A). What caused these rare axon breakages
552 is not immediately clear. On the other hand, we observed that long stretches of amyloid-
553 loaded vesicles with large spheroid formation on the axons caused dramatic dystrophy
554 to a degree that the axon morphology could no longer be recognized (Figure 8B). The
555 long stretch clustering of vesicles with spheroid formation was likely due to lysosome
556 clustering as indicated by the endosome/lysosomal marker Sortilin1 (Figure 8C). It is
557 possible that the continuous enlargement of destabilized lysosomal compartments
558 across long distance might finally result in axon breakages in some cases.
559
560

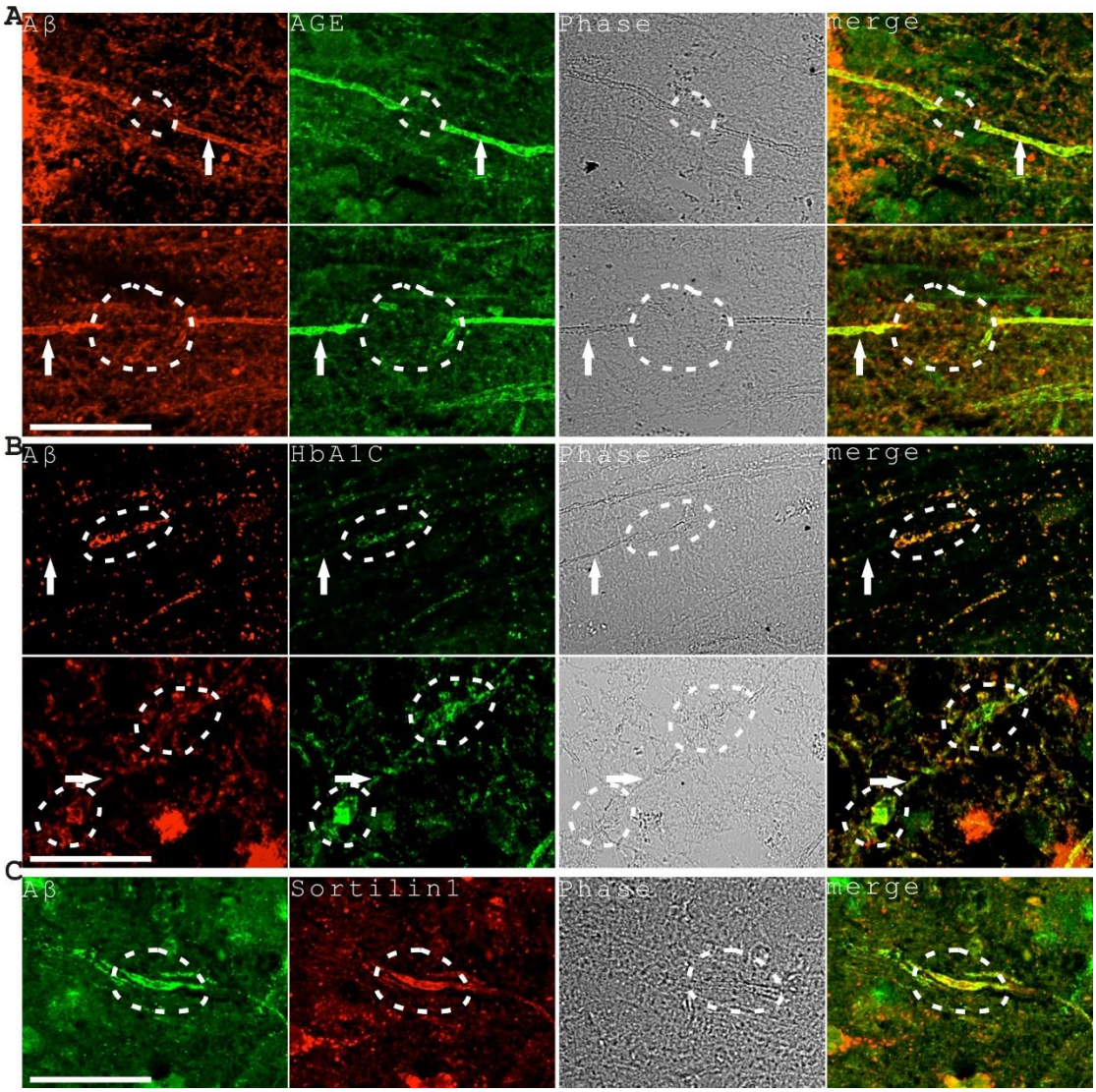

Figure 8. Under rare occasions, axon breakages were observed in AD frontal brain tissues. A. Two broken axons were identified with AGE and Aβ immunohistochemistry in AD brain tissues. The axonal gap in the top image was measured around 24.4 μm while in the bottom image was measured around 38.4 μm. The broken regions were marked with dashed lines while the parental axons were indicated with arrows. **B**. Two examples of damaged axons associated with large vesicle clusters and spheroid formation enriched for amyloid markers Aβ and HbA1C. The long stretch of clustered vesicles (indicated with dashed lines) in the top panel measured around 32.5 μm in length. The maximal width of the two large spheroids (indicated with dashed lines) in the bottom panel reached 6.2 μm (top-right position) and 8.3 μm (bottom-left position) respectively. The affected axons were indicated with arrows. **C**. A long axonal region (indicated with dashed lines) with large spheroid formation associated with

endosomal/lysosomal domains marked with Sortilin1 immunostaining. This region was measured around 26.1 μm in length. The maximal width of the spheroid measured around 4.1 μm. Scale bars, 50 μm.

Discussion:

The reason that axonal Aβ staining was not clearly observed in our previous studies[3, 9] is likely because of the relatively small size of axons and the larger and stronger senile plaque Aβ staining camouflaging the fainter staining of axonal Aβ. The widespread axonal enlargement associated with Aβ deposition might have a significant influence on AD pathology. It has been shown that in the natural animal species, axons with larger diameter have higher transduction speed, for example, in the case of the squid giant axon[33]. However, in the case of AD, the enlarged axons were not natural but instead pathological, which were filled with toxic Aβ, hemorrhagic proteins and destabilized lysosomes. In addition, lysosomal leakage can induce axonal structural damages and increase axolemmal permeability, which might further damage the myelin sheath. Both human and mouse studies indicated that axon diameter increases with aging and cognition decline[34, 35]. There is also a reduced velocity of action potential transmission in AD patients and AD-model transgenic mice[36, 37]. Diffusion tensor imaging studies also indicated that structural damage and disconnection in the white matter is prominent in AD [38, 39]. Axonal amyloidosis and enlargement in AD are likely linked to transduction velocity decrease and white matter damage phenotypes. Besides the basic axonal enlargement phenotype in AD, spheroid formation is also frequently observed. Previous studies showed that spheroid formation on axons also slows down the speed of action potential transduction[40, 41]. All these studies presented strong evidence that there are serious axonal defects in AD with transduction speed decline as a central phenotype. How and to what extent Aβ deposition in enlarged axons impacts on the whole brain connectome requires further large-scale quantitative analysis and *in vivo* animal and human studies.

Axonal amyloidosis additionally induces structural changes such as a decrease of MAP2 protein, which might be related to Aβ toxicity in inducing lysosomal destabilization. It has been shown *in vitro* that extracellular Aβ was taken up and concentrated in lysosomes and induced lysosome destabilization and permeabilization[20, 21]. Lysosome permeabilization has been studied in mouse AD models and was considered as the possible mechanism for neuronal cell death and senile plaque formation[23, 42, 43]. A previous study also identified abnormal protease-deficient lysosomes in the swollen axons surrounding senile plaques[22]. The study defined the lysosome defect as a lysosome maturation deficiency. In this study, we provided evidence that Aβ is linked to lysosome destabilization at single lysosome level and single axon level. We think that the axonal or cellular lysosomes were not intrinsically protease-deficient but rather be destabilized by Aβ and Aβ-associated hemorrhagic or vascular factors such as ApoE, Hemin, HbA1C, HBA, ACTA2 and ColIV. It is entirely possible that Aβ-associated factors are also affecting lysosome stability, maturation or lysosome pH besides Aβ itself. This study further supported our previous studies that the pathological Aβ peptide in AD tissues comes from an exogenous source, the hemorrhagic Aβ leakage, instead of coming from neurons themselves[3, 9]. Although it is possible that lysosome leakage might leads to neuronal cell death, we think lysosome leakage in the cells could illicit a complicate "lysosome leakage response" to counter-react the damaging effect of lysosome leakage. Our preliminary data did not confirm a straightforward increase of neuronal apoptosis with TUNEL assay as an apoptotic marker and MAP2 reduction as a marker for lysosome-leakage associated proteomic damage. It warrants more extensive investigations on the mechanism of "lysosome leakage response" in the future.

In our opinion, Aβ could be classified as a type of lysosomal “toxin”, which exerts its unique toxicity upon lysosomal intake and processing. The current study emphasized that lysosomal destabilization might not be due to Aβ alone since neuronal cell amyloidosis associated with the enrichment of multiple hemorrhagic or vascular markers such as ACTA2, ColIV, HBA, ApoE, HbA1C and Hemin as shown in Figure 5

634 and Figure 7, which are either major Aβ binding partners or major components of
635 microhemorrhage [3, 9, 28, 44]. It is well-known that Hemin is a neurotoxic molecule
636 by itself[45, 46]. Axonal amyloidosis also associated with Sortilin1 expression.
637 Sortilin1 is an endosome/lysosome marker that has been identified as a major receptor
638 of ApoE[31]. Axons might take up exogenous Aβ complexes through receptor-related
639 mechanisms, independent of or in conjunction with the neural soma, by the relay chains
640 starting from Aβ to ApoE then to Sortilin1. The intake of a large number of hemorrhagic
641 proteins along with Aβ could possibly induce severe axonal proteostatic stress besides
642 the toxicity effects of Aβ especially when the axon-soma connection might be
643 compromised.
644
645 Both Aβ deposition and Tau phosphorylation are important components of AD
646 pathology, however, how these two events connect is not clear. Previously, it has been
647 suggested that Aβ and Tau co-localize in AD "synaptosomes"[47]. In this study, we
648 provide another possible answer that Aβ and Tau are both connected to destabilized
649 lysosomes. There is ample evidence that Aβ endocytosis induces lysosome
650 destabilization[19, 20, 48]. There is also strong evidence that Aβ likely induces Tau
651 phosphorylation[49, 50]. We show in this study that Tau phosphorylation associates
652 with destabilized lysosomes in tangles, dystrophic neurites and also neuropil threads. It
653 is not known whether Tau phosphorylation or lysosome destabilization is the upstream
654 event. However, if taking into account for the MAP2 reduction in axons and the
655 evidence in the literature that MAP2 competes with Tau for microtubule binding[51]
656 and could prevent Tau aggregation[52], lysosomal destabilization might work upstream
657 of Tau phosphorylation by chronically degrading its competitive inhibitor MAP2. The
658 biological significance of lysosome destabilization in the neural soma in AD tissues is
659 worthy of future investigations.
660
661 Under rare occasions, the breakage of axons has been observed in a small number of
662 axons in our experiments. When axon breakages happen and are not repaired, Wallerian
663 degeneration of axons might occur, which could result in axon loss. Since axon

breakages with small gaps are difficult to detect, the actual axonal breakage events in AD brains might be more abundant than what we observed. How frequently the axonal breakages and Wallerian degeneration happen in AD brains requires further investigation. Previous *in vitro* study has shown that Aβ peptide actually induces axon degeneration precedes cell death in hippocampal neuron cell culture models[53], indicating a possible "dying back" mechanism of neuronal degeneration in AD. Both Wallerian degeneration and axon regeneration are affected by various genetic mutations[54-56]. To combat Alzheimer's disease efficiently, firstly, we need to find ways to prevent microvascular blood leakage and axonal accumulation of Aβ and hemorrhagic proteins. Secondly, treatments that can specifically slow down Wallerian degeneration and facilitate axon repair, reconnection and regeneration are also likely strongly beneficial for AD patients.

Acknowledgements: We want to thank the help from Dr. Ma Chao and Dr. Qiu Wenying for providing AD tissue sections from National Human Brain Bank for Development and Function, Chinese Academy of Medical Sciences and Peking Union Medical College, Beijing, China. Additionally, we want to thank Dr. Ming Yang from Shanghai Jiao Tong University, Dr. Xiangli Zhang from Shandong University, Dr. Peng Du and Dr. Lei Xia from Xinhua Hospital for valuable scientific discussions. Moreover, we want to thank Housheng Wang, Pingxin Liu, Xiaoyi Bao, and Jun Wang for excellent laboratory assistance.

References:

1. Hardy, J.A. and G.A. Higgins, *Alzheimer's disease: the amyloid cascade hypothesis.* Science, 1992. **256**(5054): p. 184-5.
2. Lane, C.A., J. Hardy, and J.M. Schott, *Alzheimer's disease.* European Journal of Neurology, 2018. **25**(1): p. 59-70.
3. Fu, H., et al., *Senile plaques in Alzheimer's disease arise from Aβ- and Cathepsin D-enriched mixtures leaking out during intravascular haemolysis and microaneurysm rupture.* FEBS Lett, 2023. **597**(7): p. 1007-1040.
4. Cras, P., et al., *Senile Plaque Neurites in Alzheimer-Disease Accumulate Amyloid Precursor Protein.* Proc Natl Acad Sci U S A, 1991. **88**(17): p. 7552-7556.

5. Tsai, J., et al., *Fibrillar amyloid deposition leads to local synaptic abnormalities and breakage of neuronal branches.* Nature Neuroscience, 2004. **7**(11): p. 1181-1183.
6. Braak, H. and K. Del Tredici, *Amyloid-β may be released from non-junctional varicosities of axons generated from abnormal tau-containing brainstem nuclei in sporadic Alzheimer's disease: a hypothesis.* Acta Neuropathologica, 2013. **126**(2): p. 303-306.
7. Salvadores, N., C. Gerónimo-Olvera, and F.A. Court, *Axonal Degeneration in AD: The Contribution of Aβ and Tau.* Front Aging Neurosci, 2020. **12**: p. 581767.
8. Fu, H., et al., *Persisting and Increasing Neutrophil Infiltration Associates with Gastric Carcinogenesis and E-cadherin Downregulation.* Sci Rep, 2016. **6**: p. 29762.
9. Fu, H.L., et al., *Aβ-Aggregation-Generated Blue Autofluorescence Illuminates Senile Plaques as well as Complex Blood and Vascular Pathologies in Alzheimer's Disease.* Neuroscience Bulletin, 2024.
10. Katsuki, H. and M. Hijioka, *Intracerebral Hemorrhage as an Axonal Tract Injury Disorder with Inflammatory Reactions.* Biological & Pharmaceutical Bulletin, 2017. **40**(5): p. 564-568.
11. Dowson, J.H., *A sensitive method for the demonstration of senile plaques in the dementing brain.* Histopathology, 1981. **5**(3): p. 305-10.
12. Gao, Y., et al., *Imaging and Spectral Characteristics of Amyloid Plaque Autofluorescence in Brain Slices from the APP/PS1 Mouse Model of Alzheimer's Disease.* Neurosci Bull, 2019. **35**(6): p. 1126-1137.
13. Dajas-Ballador, F., E.V. Jones, and A.J. Whitmarsh, *The JIP1 scaffold protein regulates axonal development in cortical neurons.* Current Biology, 2008. **18**(3): p. 221-226.
14. Pinatel, D., et al., *Inhibitory axons are targeted in hippocampal cell culture by anti-Caspr2 autoantibodies associated with limbic encephalitis.* Frontiers in Cellular Neuroscience, 2015. **9**.
15. Li, R.W., et al., *Cattle encephalon glycoside and ignotin reduced white matter injury and prevented post-hemorrhagic hydrocephalus in a rat model of intracerebral hemorrhage.* Scientific Reports, 2016. **6**.
16. Liu, X.Y., et al., *3D printing of injury-preconditioned secretome/collagen/heparan sulfate scaffolds for neurological recovery after traumatic brain injury in rats.* Stem Cell Research & Therapy, 2022. **13**(1).
17. Lee, E.J., et al., *Three-dimensional visualization of cerebral blood vessels and neural changes in thick ischemic rat brain slices using tissue clearing.* Scientific Reports, 2022. **12**(1).
18. Gumy, L.F., et al., *MAP2 Defines a Pre-axonal Filtering Zone to Regulate KIF1-versus KIF5-Dependent Cargo Transport in Sensory Neurons.* Neuron, 2017. **94**(2): p. 347-+.
19. Takahashi, R.H., et al., *Intraneuronal Alzheimer abeta42 accumulates in multivesicular bodies and is associated with synaptic pathology.* The American journal of pathology, 2002. **161 5**: p. 1869-79.
20. Liu, R.Q., et al., *Membrane localization of beta-amyloid 1-42 in lysosomes: a possible mechanism for lysosome labilization.* J Biol Chem, 2010. **285**(26): p. 19986-96.
21. Zaretsky, D.V., M.V. Zaretskaia, and Y.I. Molkov, *Membrane channel hypothesis of lysosomal permeabilization by beta-amyloid.* Neurosci Lett, 2022. **770**: p. 136338.
22. Gowrishankar, S., et al., *Massive accumulation of luminal protease-deficient axonal*

lysosomes at Alzheimer's disease amyloid plaques. Proc Natl Acad Sci U S A, 2015. **112**(28): p. E3699-708.

23. Lee, J.-H., et al., *Faulty autolysosome acidification in Alzheimer's disease mouse models induces autophagic build-up of Aβ in neurons, yielding senile plaques.* Nature Neuroscience, 2022. **25**(6): p. 688-701.
24. Cullen, K.M., Z. Kócsi, and J. Stone, *Pericapillary Haem-Rich Deposits: Evidence for Microhaemorrhages in Aging Human Cerebral Cortex.* Journal of Cerebral Blood Flow & Metabolism, 2005. **25**(12): p. 1656-1667.
25. Cullen, K.M., Z. Kocsi, and J. Stone, *Microvascular pathology in the aging human brain: Evidence that senile plaques are sites of microhaemorrhages.* Neurobiology of Aging, 2006. **27**(12): p. 1786-1796.
26. Hecht, M., et al., *Capillary cerebral amyloid angiopathy in Alzheimer's disease: association with allocortical/hippocampal microinfarcts and cognitive decline.* Acta Neuropathol, 2018. **135**(5): p. 681-694.
27. Stone, J., *What initiates the formation of senile plaques? The origin of Alzheimer-like dementias in capillary haemorrhages.* Med Hypotheses, 2008. **71**(3): p. 347-59.
28. Chuang, J.Y., et al., *Interactions between amyloid-β and hemoglobin: implications for amyloid plaque formation in Alzheimer's disease.* PLoS One, 2012. **7**(3): p. e33120.
29. Miyakawa, T., et al., *The Relationship between Senile Plaques and Cerebral Blood-Vessels in Alzheimers-Disease and Senile Dementia - Morphological Mechanism of Senile Plaque Production.* Virchows Archiv B-Cell Pathology Including Molecular Pathology, 1982. **40**(2): p. 121-129.
30. Bu, X.L., et al., *Blood-derived amyloid-β protein induces Alzheimer's disease pathologies.* Molecular Psychiatry, 2018. **23**(9).
31. Carlo, A.S., et al., *The pro-neurotrophin receptor sortilin is a major neuronal apolipoprotein E receptor for catabolism of amyloid-β peptide in the brain.* J Neurosci, 2013. **33**(1): p. 358-70.
32. Hu, X., et al., *Sortilin Fragments Deposit at Senile Plaques in Human Cerebrum.* Front Neuroanat, 2017. **11**: p. 45.
33. Hartline, D.K. and D.R. Colman, *Rapid conduction and the evolution of giant axons and myelinated fibers.* Curr Biol, 2007. **17**(1): p. R29-35.
34. Fan, Q., et al., *Age-related alterations in axonal microstructure in the corpus callosum measured by high-gradient diffusion MRI.* NeuroImage, 2019. **191**: p. 325-336.
35. Parandavar, E., et al., *Long-term demyelination and aging-associated changes in mice corpus callosum; evidence for the role of accelerated aging in remyelination failure in a mouse model of multiple sclerosis.* Aging Cell, 2024. **n/a**(n/a): p. e14211.
36. Qian, X., et al., *Reduced Peripheral Nerve Conduction Velocity is Associated with Alzheimer's Disease: A Cross-Sectional Study from China.* Neuropsychiatr Dis Treat, 2022. **18**: p. 231-242.
37. Gelman, S., J. Palma, and A. Ghavami, *Axonal Conduction Velocity in CA1 Area of Hippocampus is Reduced in Mouse Models of Alzheimer's Disease.* J Alzheimers Dis, 2020. **77**(4): p. 1383-1388.
38. Chen, Y., et al., *Abnormal white matter changes in Alzheimer's disease based on diffusion tensor imaging: A systematic review.* Ageing Research Reviews, 2023. **87**: p. 101911.

39. Fellgiebel, A. and I. Yakushev, *Diffusion tensor imaging of the hippocampus in MCI and early Alzheimer's disease.* J Alzheimers Dis, 2011. **26 Suppl 3**: p. 257-62.
40. Kolaric, K.V., et al., *Focal axonal swellings and associated ultrastructural changes attenuate conduction velocity in central nervous system axons: a computer modeling study.* Physiol Rep, 2013. **1**(3): p. e00059.
41. Yuan, P., et al., *PLD3 affects axonal spheroids and network defects in Alzheimer's disease.* Nature, 2022. **612**(7939): p. 328-337.
42. Nixon, R.A., et al., *Extensive involvement of autophagy in Alzheimer disease: An immuno-electron microscopy study.* Journal of Neuropathology and Experimental Neurology, 2005. **64**(2): p. 113-122.
43. Nixon, R.A., *Autophagy-lysosomal-associated neuronal death in neurodegenerative disease.* Acta Neuropathologica, 2024. **148**(1).
44. Golabek, A., et al., *Amyloid β binding proteins in vitro and in normal human cerebrospinal fluid.* Neuroscience Letters, 1995. **191**(1): p. 79-82.
45. Dang, T.N., et al., *Uptake, metabolism and toxicity of hemin in cultured neurons.* Neurochem Int, 2011. **58**(7): p. 804-11.
46. Robinson, S.R., et al., *Hemin toxicity: a preventable source of brain damage following hemorrhagic stroke.* Redox Rep, 2009. **14**(6): p. 228-35.
47. Fein, J.A., et al., *Co-localization of amyloid beta and tau pathology in Alzheimer's disease synaptosomes.* Am J Pathol, 2008. **172**(6): p. 1683-92.
48. Tam, J.H.K., C. Seah, and S.H. Pasternak, *The Amyloid Precursor Protein is rapidly transported from the Golgi apparatus to the lysosome and where it is processed into beta-amyloid.* Molecular Brain, 2014. **7**(1): p. 54.
49. Zheng, W.H., et al., *Amyloid beta peptide induces tau phosphorylation and loss of cholinergic neurons in rat primary septal cultures.* Neuroscience, 2002. **115**(1): p. 201-11.
50. Mattsson-Carlgren, N., et al., *Aβ deposition is associated with increases in soluble and phosphorylated tau that precede a positive Tau PET in Alzheimer's disease.* Sci Adv, 2020. **6**(16): p. eaaz2387.
51. Sandoval, I.V. and J.S. Vandekerckhove, *A comparative study of the in vitro polymerization of tubulin in the presence of the microtubule-associated proteins MAP2 and tau.* J Biol Chem, 1981. **256**(16): p. 8795-800.
52. Holden, M.R., et al., *MAP2 caps tau fibrils and inhibits aggregation.* J Biol Chem, 2023. **299**(7): p. 104891.
53. Alobuia, W.M., W. Xia, and B.P. Vohra, *Axon degeneration is key component of neuronal death in amyloid-β toxicity.* Neurochem Int, 2013. **63**(8): p. 782-9.
54. Coleman, M.P. and M.R. Freeman, *Wallerian degeneration, wld(s), and nmnat.* Annu Rev Neurosci, 2010. **33**: p. 245-67.
55. Teoh, J.S., et al., *Bridging the gap: axonal fusion drives rapid functional recovery of the nervous system.* Neural Regen Res, 2018. **13**(4): p. 591-594.
56. Neumann, B., et al., *Axonal regeneration proceeds through specific axonal fusion in transected C. elegans neurons.* Dev Dyn, 2011. **240**(6): p. 1365-72.

Supplementary Information for

Pathological axonal enlargement in connection with amyloidosis, lysosome destabilization and hemorrhage is a major defect in Alzheimer's disease

Hualin Fu, Jilong Li, Chunlei Zhang, Guo Gao, Qiqi Ge, Xinping Guan, Daxiang Cui

This PDF file includes:

Supplementary Fig. 1 to 11

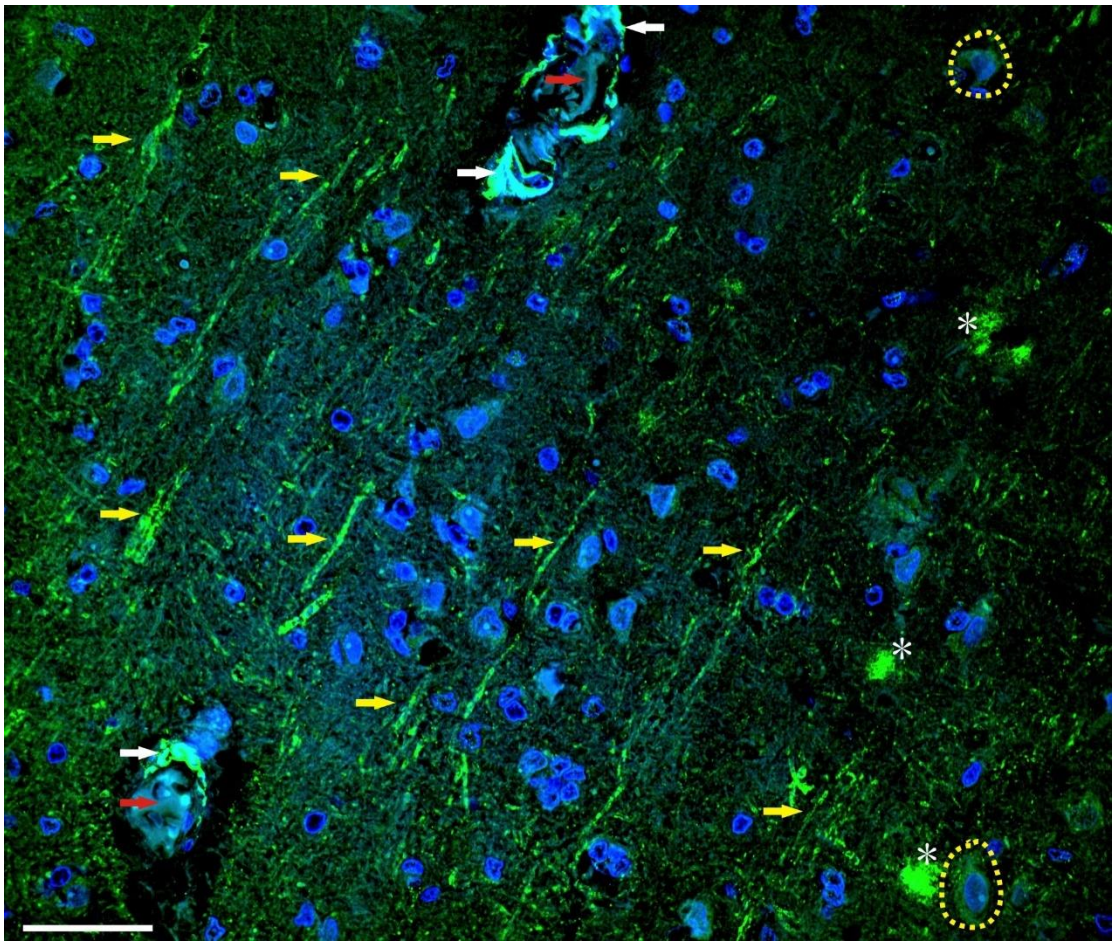

Supplementary Figure 1. An overview picture indicated that Aβ expressed in axon bundles, senile plaques, CAA blood vessel walls, the blood vessel lumen and also in neurons in AD frontal brain tissues. Aβ was stained with green fluorescence and the nuclei labeled blue by DAPI. The yellow arrows indicated axon bundles, while white arrows indicated CAA blood vessels and the red arrows indicated the blood vessel lumens. Many indicated axons showed quite even enlargement of the axons. A few small senile plaques were indicated with asterisks and Aβ expression in neurons was indicated with yellow dashed circles. Scale bar, 50 μm.

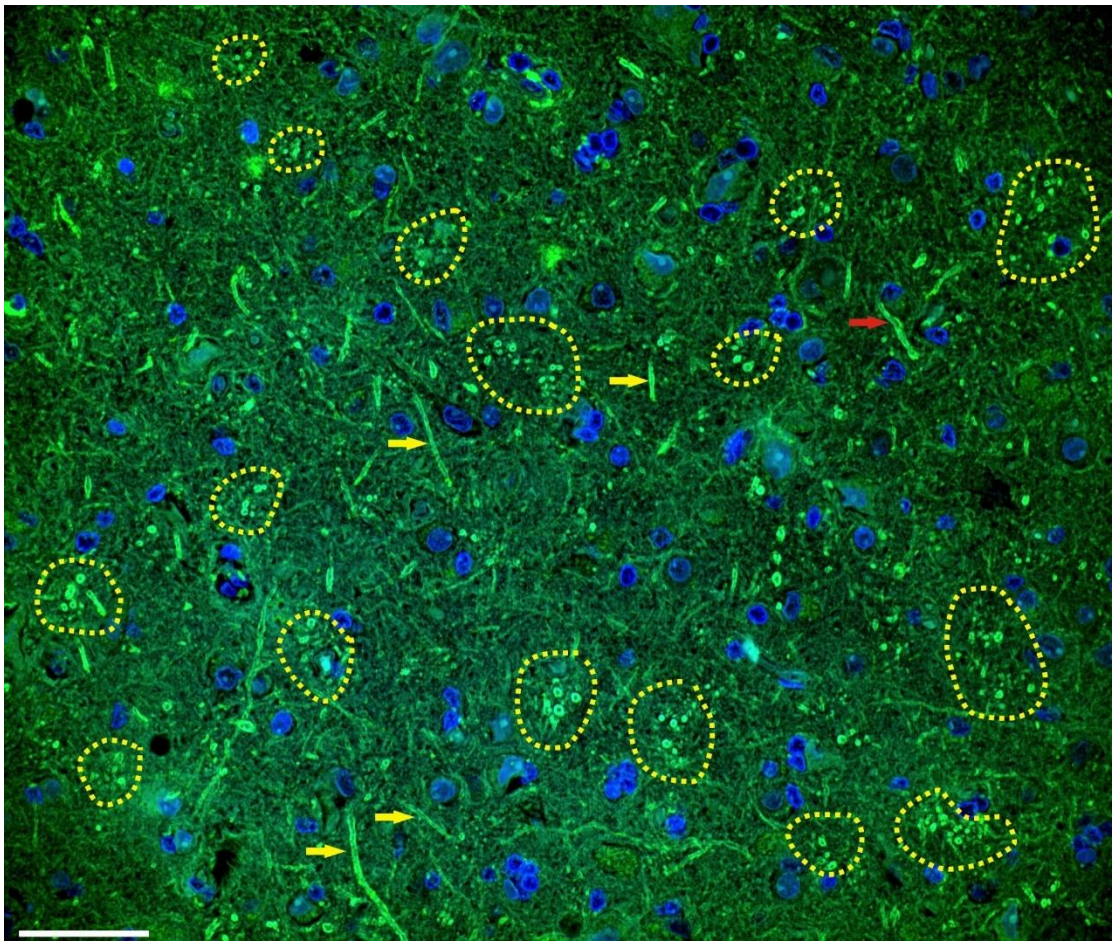

Supplementary Figure 2. An overview picture illustrated many axon bundles with Aβ-positive axons in a transverse orientation in AD frontal brain tissues. Aβ was stained with green fluorescence and the nuclei labeled blue by DAPI. The yellow dashed circles indicated the axon bundles. Many axons at the longitudinal direction showed quite even enlargement of the axons as indicated with yellow arrows. An axon with spheroid formation was indicated with a red arrow. There are around 8.44±4.10 Aβ-positive axons on average in each axon bundle (N=16). Scale bar, 50 μm.

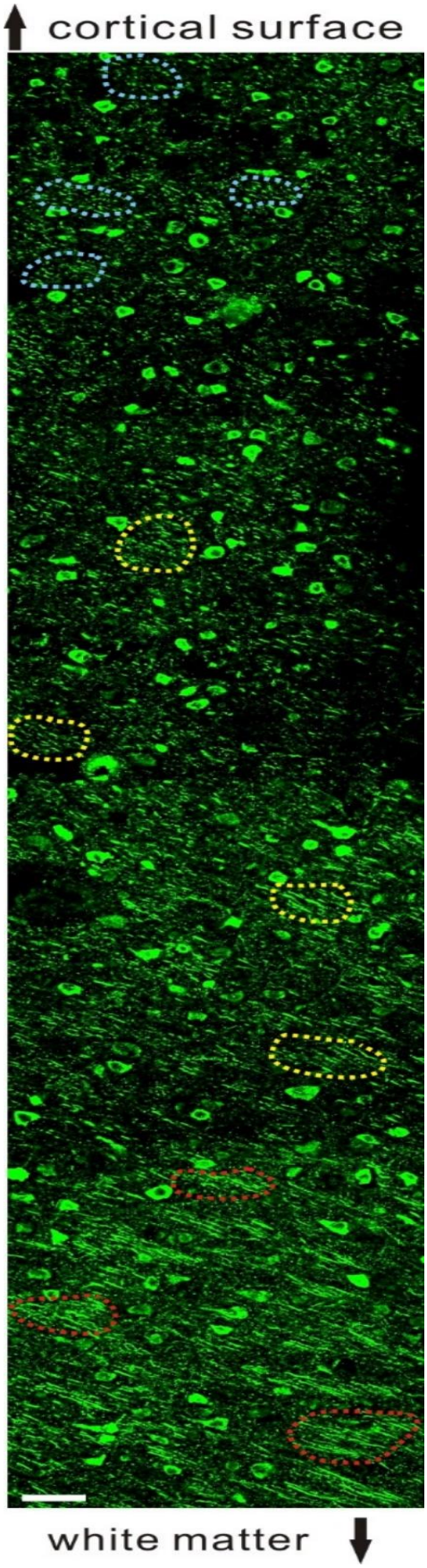

Supplementary Figure 3. MAP2 antibody labeled intracortical axon bundles clearly in control frontal brain tissues. The orientation of this tissue slide is from the cortical

surface (top) to the white matter (bottom). Axon bundles at both transverse (top, indicated with blue circles) and longitudinal orientation (bottom, indicated with red circles) could be observed in the same pathological section at different depth in the brain tissues. Axon bundles with intermediate length axon fragments could be observed in between (indicated with yellow circles). Not all but only representative axon bundles were indicated. These axon bundles has an average diameter of 61.61±9.88 um (N=11). Each bundle contains an average of 19.09±4.61 axons (N=11). Scale bar, 50 μm.

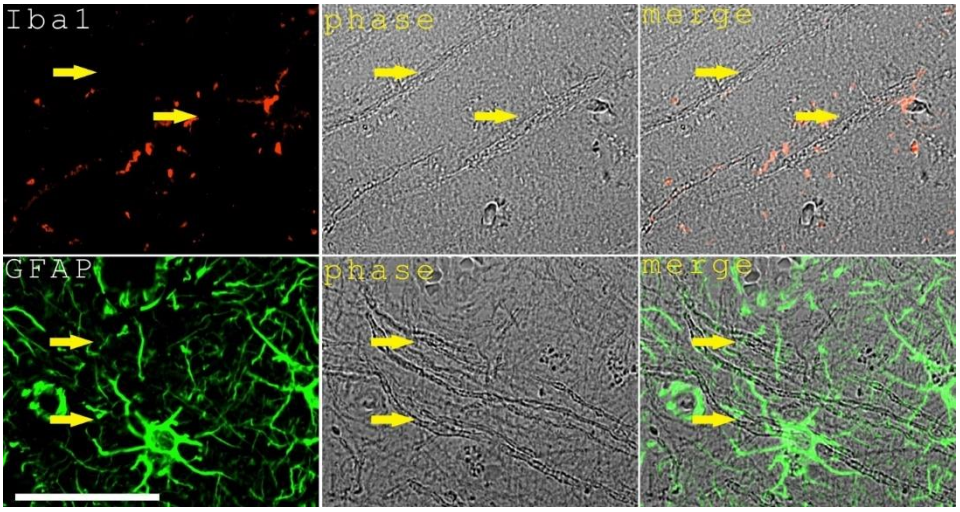

Supplementary Figure 4. Enlarged axons in AD frontal brain tissues were not stained with microglial marker Iba1 (top panel with red fluorescence) or astroglia marker GFAP (bottom panel with green fluorescence) although contacts between microglial cells or astrocytes and these axons were observed. The enlarged axons were indicated with yellow arrows and were clearly identifiable with phase contrast microscopy. Scale bar, 50 μm.

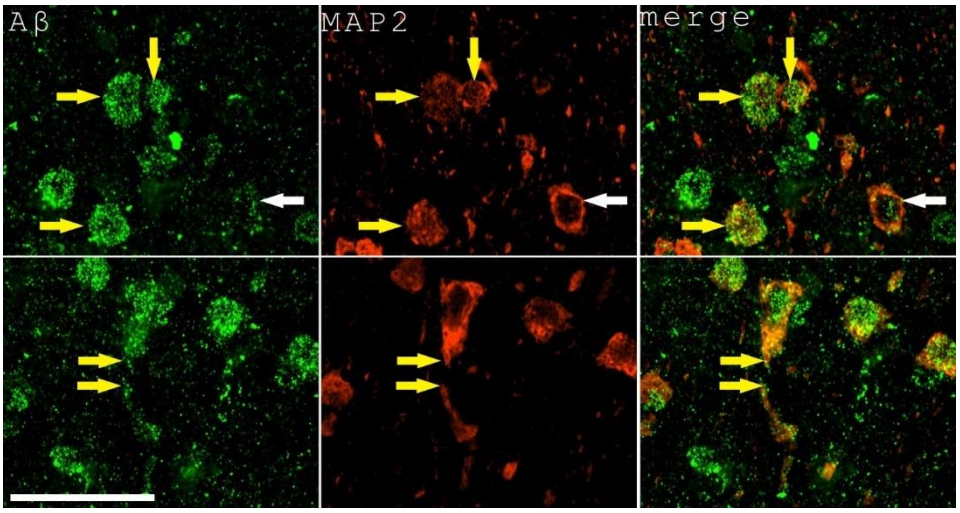

Supplementary Figure 5. Intracellular Aβ associates with the decrease of MAP2 expression in neurons in AD frontal brain tissues. Aβ was labeled with green fluorescence while MAP2 was labeled with red fluorescence. The top panel indicates several neurons (indicated with yellow arrows) with abundant intracellular Aβ had reduced MAP2 staining comparing to a control neuron with little intracellular Aβ (indicated with a white arrow). The bottom panel showed an abrupt loss of MAP2 expression in a proximal axon neighboring region in a large pyramid neuron (indicated with yellow arrows). Scale bar, 50 μm.

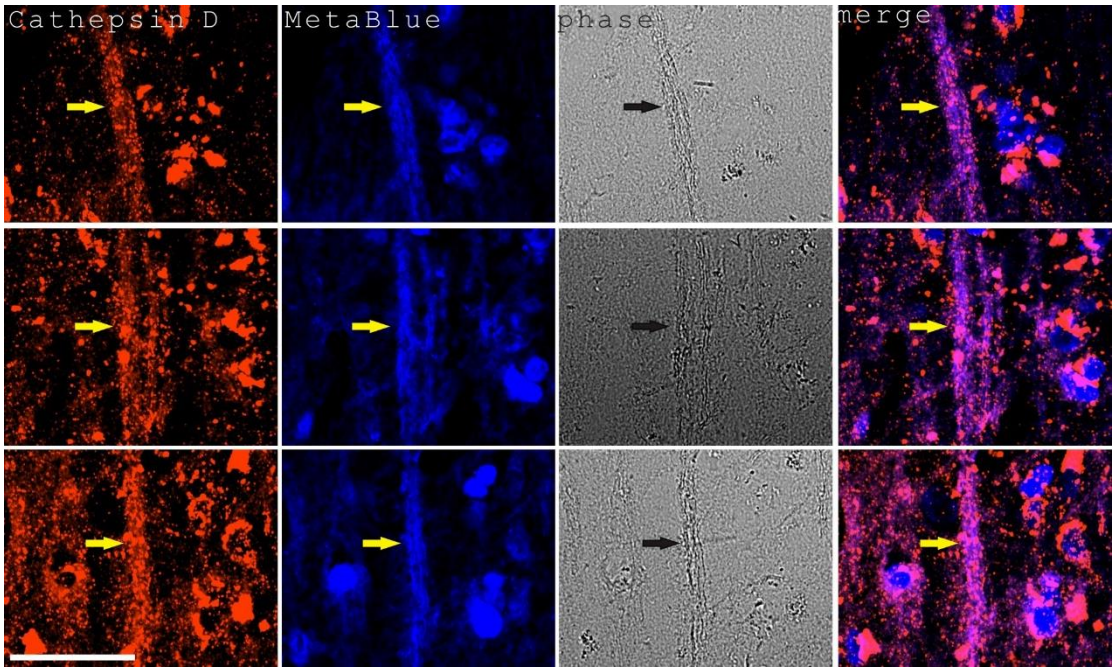

Supplementary Figure 6. Axon amyloidosis associated with fragmented, very diffusive staining of lysosome marker Cathepsin D in AD frontal brain tissues. Cathepsin D was labeled with red fluorescence while amyloid blue autofluorescence (MetaBlue) was used as a marker for axon amyloidosis. This section was also stained with DAPI to show the nuclear staining. Three representative images were shown. The arrows indicated axon bundles with amyloidosis and very diffusive Cathepsin D staining. Scale bar, 50 μm.

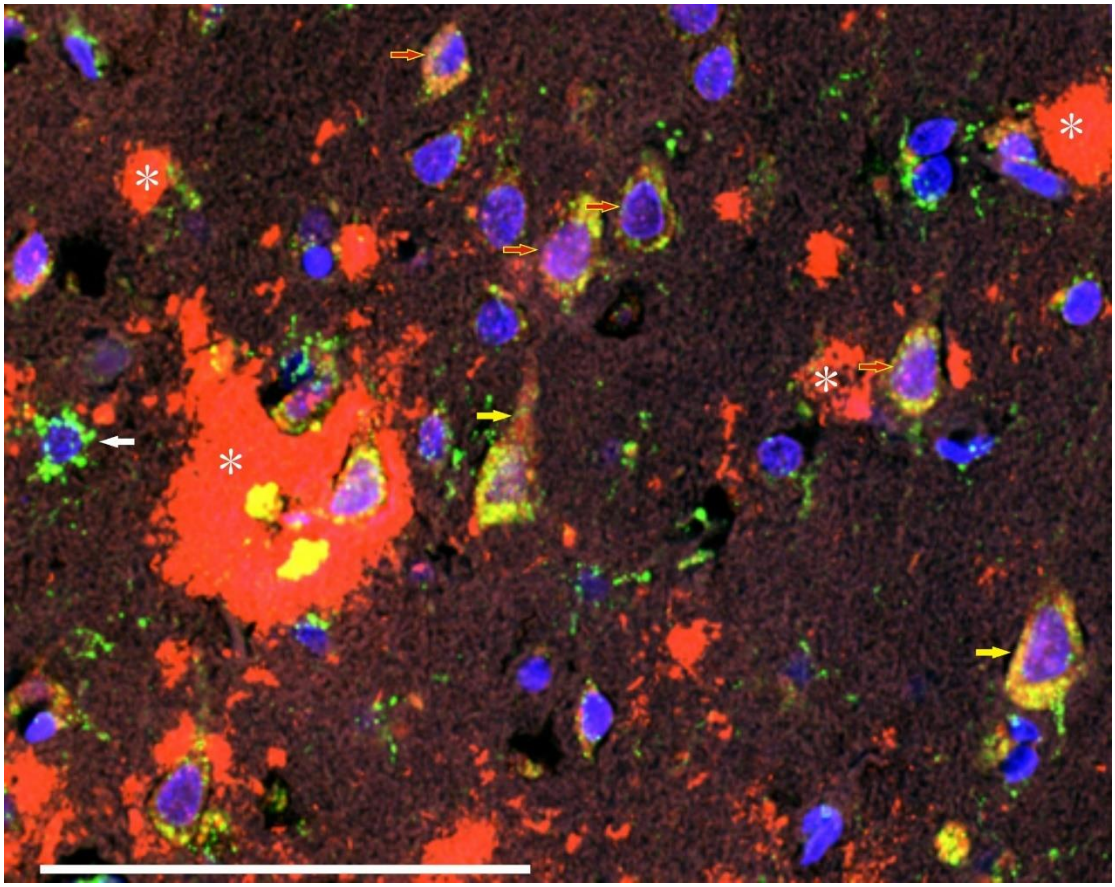

Supplementary Figure 7. A representative overview image of Aβ and Cathepsin D expression in neural cells in AD frontal brain tissues. Aβ was stained in red fluorescence while Cathepsin D was stained in green. The nuclei was labeled in blue with DAPI. Two large pyramid neurons were indicated with yellow arrows, with the left one showing abundant Aβ staining in the somatic region extending to the proximal axon. A likely astral glial cell was indicated with the white arrow as the Cathepsin D staining

indicated the outspreading astral processes. Several senile plaques were indicated with asterisks. Several other type neural cells were indicated with red arrows showing Aβ and Cathepsin D staining signals. Scale bar, 100 μm.

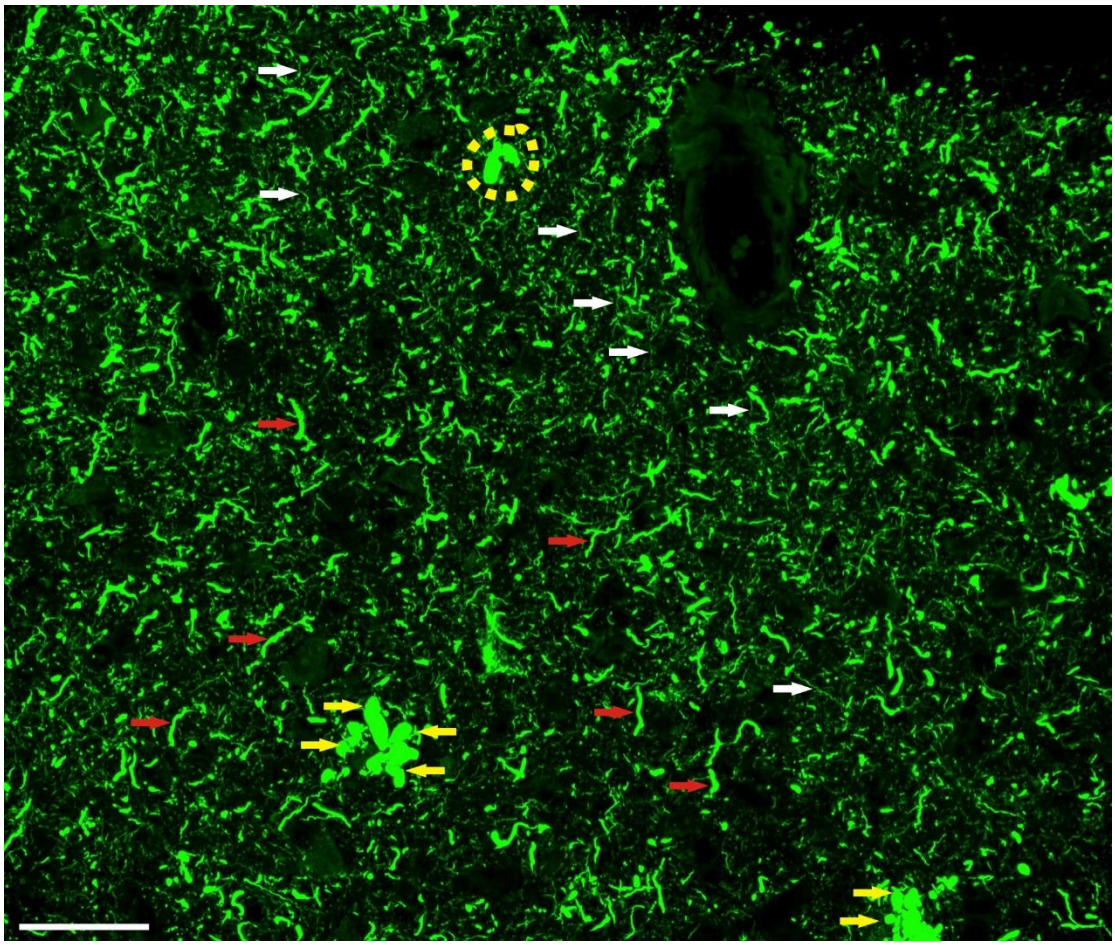

Supplementary Figure 8. Tau phosphorylation antibody stained abundant dystrophic neurites widely distributed in AD frontal brain tissues, not restricted to dystrophic neurites surrounding the senile plaques and tangled neurons. Senile plaque dystrophic neurites labeled with green fluorescence by phos-Tau antibody were indicated with yellow arrows. A tangled neuron was indicated with a yellow dashed circle. Widely distributed dystrophic neurites were indicated with red arrows. Secondary, much smaller dystrophic neurites were indicated with white arrows. Primary dystrophic neurites had an average diameter of 1.56±0.37 μm (N=40) and secondary dystrophic neurites had an average diameter of 0.40±0.09 μm (N=30). Scale bar, 50 μm.

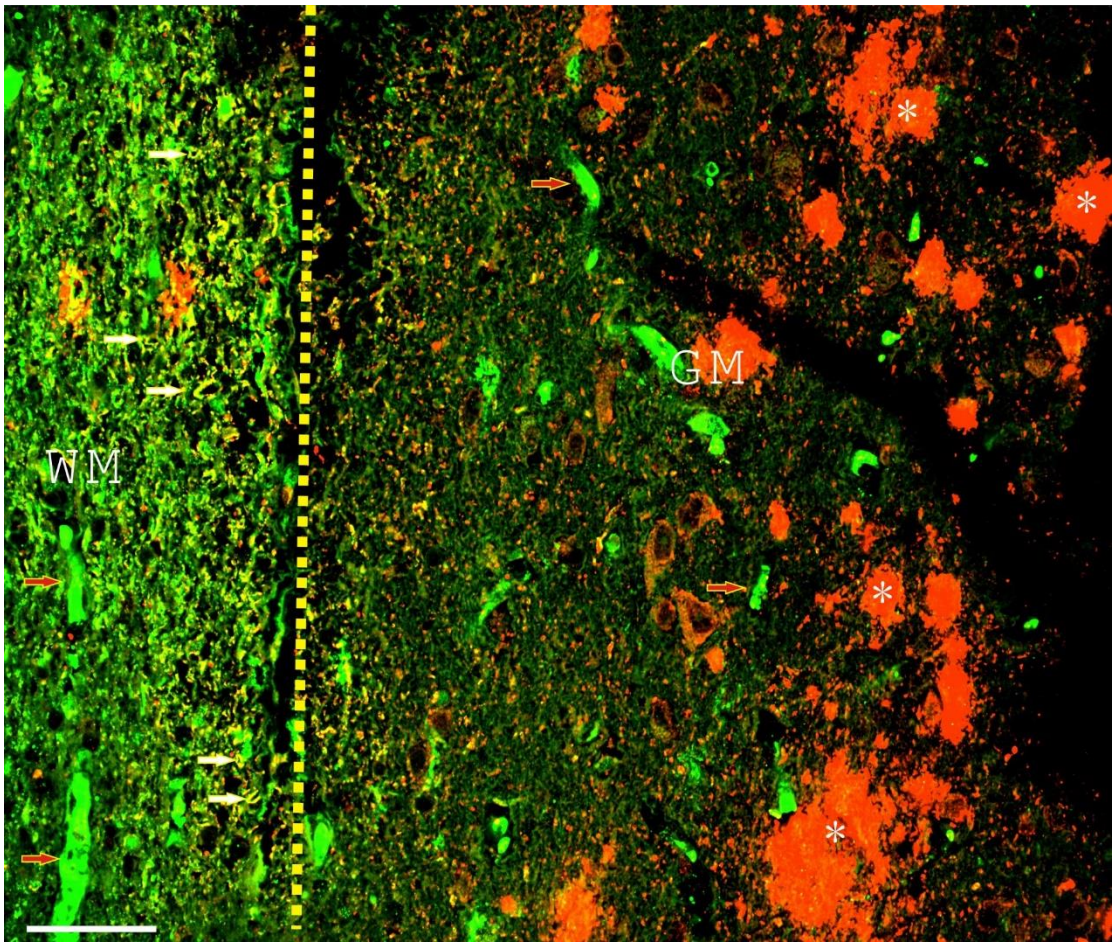

Supplementary Figure 9. An overview image of HBA and Aβ staining in AD frontal brain sections showing abundant HBA accumulation in the brain white matter axons (HBA labeled green while Aβ labeled red). Yellow dashed lines showed the separation between grey matter (on the right) and white matter (on the left). Blood vessels in white matter and grey matter were all clearly labeled with red blood cell marker HBA (indicated with red arrows). At the same time, strong signals in the white matter axons were observed (some representative axons were indicated with white arrows). Senile plaques were marked with asterisks. WM, white matter. GM, grey matter. Scale bar, 50 μm.

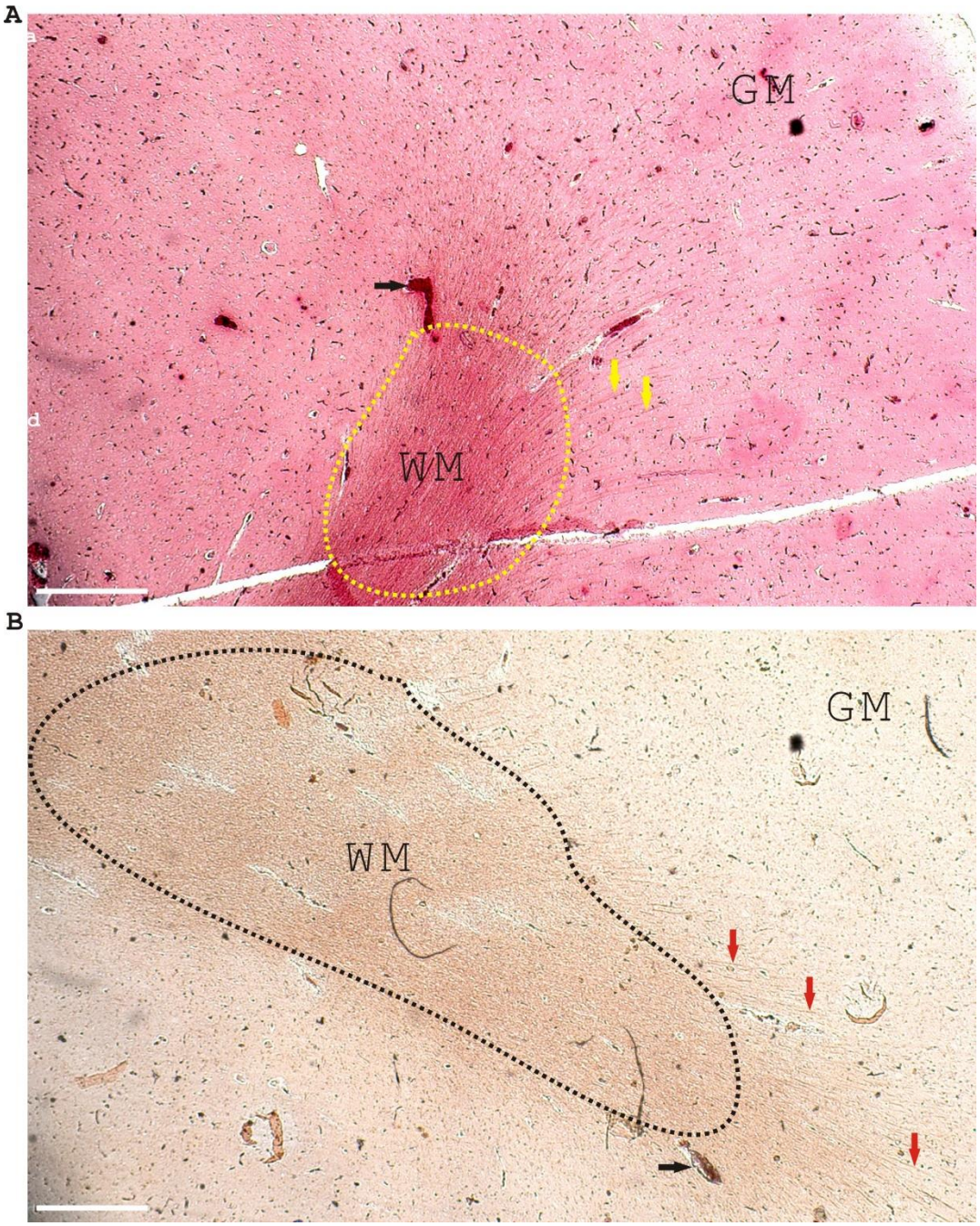

Supplementary Figure 10: Many axons were positively stained by Alizarin Red and Rhodanine in AD frontal brain tissues. **A.** This panel showed that Alizarin red positively stained the blood cells in the blood vessels (a representative blood vessel was indicated with a black arrow) and the axons (indicated with yellow arrows). Alizarin red stained the white matter (WM) (indicated with yellow dashed circles) clearly while there was less staining in the grey matter (GM). **B.** This panel showed that Rhodanine positively stained the blood cells in the blood vessels (a representative blood vessel was indicated

with a black arrow) and the axons (indicated with red arrows). The white matter was also labeled with Rhodanine broadly (indicated with black dashed circles). GM, grey matter. WM, white matter. Scale bar, 500 μm.

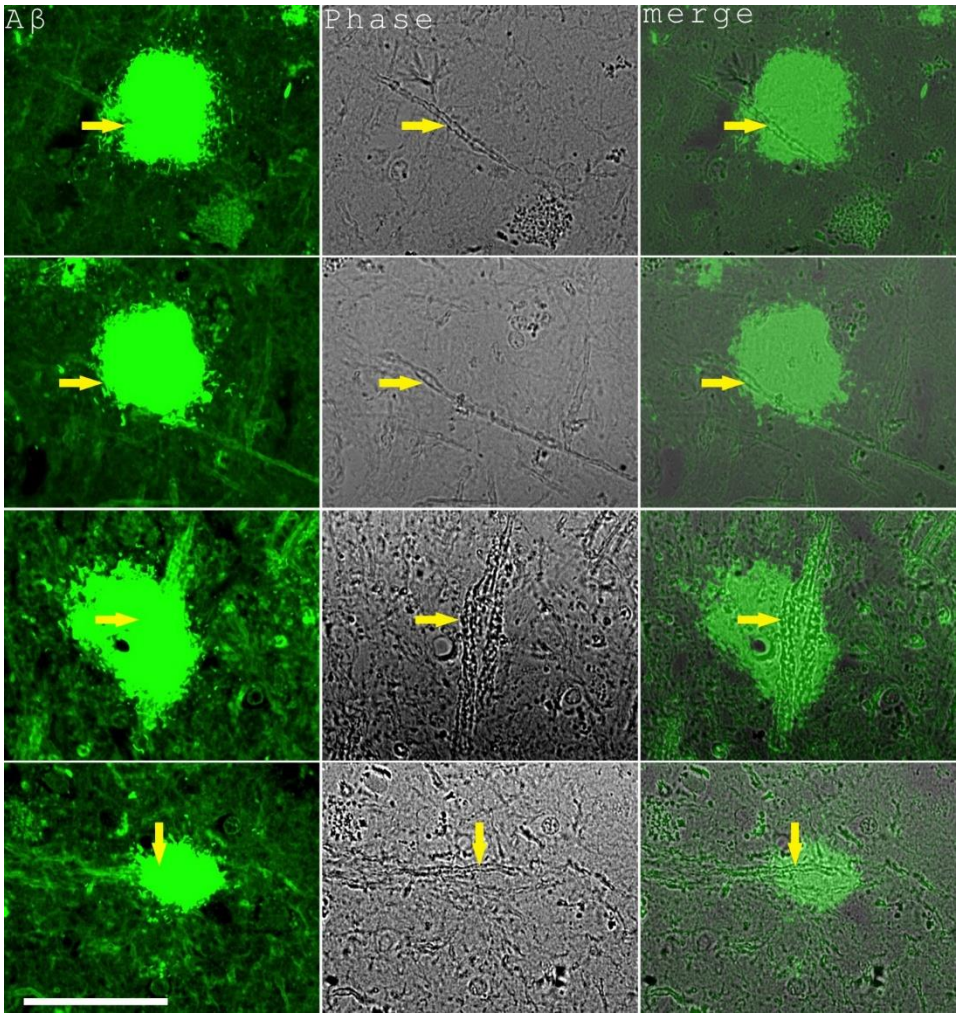

Supplementary Figure 11. Enlarged axons (indicated with arrows) were detected inside of senile plaques in AD frontal brain tissues but axon breakage was not readily observed. Four representative images were shown. Scale bar, 50 μm.